study, vagal stimulation at 20-Hz lowered the HR by approximately 200 beats/min (to less than 40% of the control value) but the stimulation-induced ACh release did not exceed the ischemia-induced ACh release (Figs. 1 and 3). On the other hand, vagal stimulation that reduced the HR by only 10% produces a significant increase in the survival rate of chronic heart failure rats (Li et al. 2004). Therefore, vagal stimulation probably exerts its beneficial effects not only within the ischemic region but also outside of this region. For instance, vagal stimulation in dogs with a healed myocardial infarction is known to prevent lethal arrhythmia induced by exercise (Vanoli et al. 1991). Afferent vagal activation may also contribute to the cardioprotective effects. Further studies are clearly needed to identify the mechanisms underlying the vagally induced cardioprotective effects against myocardial infarction and chronic heart failure.

Conclusion

The present study demonstrated the presence of vagal innervation in the rabbit left ventricle. Acute myocardial ischemia significantly increased the myocardial interstitial ACh levels. In addition, a brief ischemic event (5 min) caused detectable increases in ACh levels, indicating that endogenous ACh release may provide a trigger for ischemic preconditioning.

Acknowledgments

This study was supported by the Health and Labour Sciences Research Grants (H18-nano-Ippan-003, H19-nano-Ippan-009, H20-katsudo-Shitei-007, and H21-nano-Ippan-005) from the Ministry of Health, Labour and Welfare of Japan; by a Grant-in-Aid for Scientific Research (No. 20390462) from the Ministry of Education, Culture, Sports, Science and Technology of Japan; and by the Industrial Technology Research Grant Program from the New Energy and Industrial Technology Development Organization (NEDO) of Japan.

References

Akiyama T, Yamazaki T, Ninomiya I. In vivo detection of endogenous acetylcholine release in cat ventricles. American Journal of Physiology 266 (3 Pt 2), H854–H860, 1994.

Brown OM. Cat heart acetylcholine: Structural proof and distribution. American Journal of Physiology 231 (3), 781–785, 1976.

Cason BA, Gamperl AK, Slocum RE, Hickey RF. Anesthetic-induced preconditioning: Previous administration of isoflurane decreases myocardial infarct size in rabbits. Anesthesiology 87 (5), 1182–1190, 1997.

Cohen MV, Liu GS, Downey JM. Preconditioning causes improved wall motion as well as smaller infarcts after transient coronary occlusion in rabbits. Circulation 84 (1), 341–349, 1991.

Glantz SA. Primer of Biostatistics, 5th ed. McGraw-Hill, New York, 2002.

Kawada T, Yamazaki T, Akiyama T, Sato T, Shishido T, Inagaki M, Takaki H, Sugimachi M, Sunagawa K. Differential acetylcholine release mechanisms in the ischemic and non-ischemic myocardium. Journal of Molecular and Cellular Cardiology 32 (3), 405–414, 2000.

Kawada T, Yamazaki T, Akiyama T, Shishido T, Inagaki M, Uemura K, Miyamoto T, Sugimachi M, Takaki H, Sunagawa K. In vivo assessment of acetylcholine releasing function at cardiac vagal nerve terminals. American Journal of Physiology. Heart and Circulatory Physiology 281 (1), H139–H145, 2001.

Kawada T, Yamazaki T, Akiyama T, Mori H, Inagaki M, Shishido T, Takaki H, Sugimachi M, Sunagawa K. Effects of brief ischaemia on myocardial acetylcholine and noradrenaline levels in anaesthetized cats. Autonomic Neuroscience: Basic and Clinical 95 (1–2), 37–42, 2002.

Kawada T, Yamazaki T, Akiyama T, Li M, Ariumi H, Mori H, Sunagawa K, Sugimachi M. Vagal stimulation suppresses ischemia-induced myocardial interstitial norepinephrine release. Life Sciences 78 (8), 882–887, 2006a.

Kawada T, Yamazaki T, Akiyama T, Uemura K, Kamiya A, Shishido T, Mori H, Sugimachi M. Effects of Ca^{2+} channel antagonists on nerve stimulation-induced and ischemia-induced myocardial interstitial acetylcholine release in cats. American Journal of Physiology. Heart and Circulatory Physiology 291 (5), H2187–H2191, 2006b.

Kawada T, Yamazaki T, Akiyama T, Shishido T, Shimizu S, Mizuno M, Mori H, Sugimachi M. Regional difference in ischaemia-induced myocardial interstitial noradrenaline and acetylcholine releases. Autonomic Neuroscience: Basic and Clinical 137 (1–2), 44–50, 2007.

Kawada T, Yamazaki T, Akiyama T, Kitagawa H, Shimizu S, Mizuno M, Li M, Sugimachi M. Vagal stimulation suppresses ischemia-induced myocardial interstitial myoglobin release. Life Sciences 83 (13–14), 490–495, 2008.

Kilbinger H, Löffelholz K. The isolated perfused chicken heart as a tool for studying acetylcholine output in the absence of cholinesterase inhibition. Journal of Neural Transmission 38, 9–14, 1976.

Kitagawa H, Yamazaki T, Akiyama T, Sugimachi M, Sunagawa K, Mori H. Microdialysis separately monitors myocardial interstitial myoglobin during ischemia and reperfusion. American Journal of Physiology Heart and Circulatory Physiology 289 (2), H924–H930, 2005.

Krieg T, Qin Q, Philipp S, Alexeyev MF, Cohen MV, Downey JM. Acetylcholine and bradykinin trigger preconditioning in the heart through a pathway that induces Akt and NOS. American Journal of Physiology. Heart and Circulatory Physiology 287 (6), H2606–H2611, 2004.

Li M, Zheng C, Sato T, Kawada T, Sugimachi M, Sunagawa K. Vagal nerve stimulation markedly improves long-term survival after chronic heart failure in rats. Circulation 109 (1), 120–124, 2004.

Liu GS, Thornton J, Van Winkle DM, Stanley AW, Olsson RA, Downey JM. Protection against infarction afforded by preconditioning is mediated by A_1 adenosine receptors in rabbit heart. Circulation 84 (1), 350–356, 1991.

Matsuura W, Sugimachi M, Kawada T, Sato T, Shishido T, Miyano H, Nakahara T, Ikeda Y, Alexander Jr J, Sunagawa K. Vagal stimulation decreases left ventricular contractility mainly through negative chronotropic effect. American Journal of Physiology 273 (2 Pt 2), H534–H539, 1997.

Murry CE, Jennings RB, Reimer KA. Preconditioning with ischemia: A delay of lethal cell injury in ischemic myocardium. Circulation 74 (5), 1124–1136, 1986.

Nakayama Y, Miyano H, Shishido T, Inagaki M, Kawada T, Sugimachi M, Sunagawa K. Heart rate-independent vagal effect on end-systolic elastance of the canine left ventricle under various levels of sympathetic tone. Circulation 104 (19), 2277–2279, 2001.

Piper HM, Abdallah Y, Schäfer C. The first minutes of reperfusion: A window of opportunity for cardioprotection. Cardiovascular Research 61 (3), 365–371, 2004.

Przyklenk K, Kloner RA. Low-dose iv acetylcholine acts as a "preconditioning-mimetic" in the canine model. Journal of Cardiac Surgery 10 (4), 389–395, 1995.

Qin Q, Downey JM, Cohen MV. Acetylcholine but not adenosine triggers preconditioning through PI3-kinase and a tyrosine kinase. American Journal of Physiology. Heart and Circulatory Physiology 284 (2), H727–H734, 2003.

Richard V, Blanc T, Kaeffer N, Tron C, Thuillez C. Myocardial and coronary endothelial protective effects of acetylcholine after myocardial ischaemia and reperfusion in rats: Role of nitric oxide. British Journal of Pharmacology 115 (8), 1532–1538, 1995.

Shimizu S, Akiyama T, Kawada T, Shishido T, Yamazaki T, Kamiya A, Mizuno M, Sano S, Sugimachi M. In vivo direct monitoring of vagal acetylcholine release to the sinoatrial node. Autonomic Neuroscience: Basic and Clinical 148 (1–2), 44–49, 2009.

Snedecor GW, Cochran WG. Statistical Methods. Iowa State, Iowa, pp. 290–291, 1989.

Ståhle L. The use of microdialysis in pharmacokinetics and pharmacodynamics. In: Robinson, TE, JusticeJr. Jr, JB (Eds.), Microdialysis in the Neurosciences, pp. 155–174. Elsevier Science Ltd. New York, 1991.

Thames MD, Klopfenstein HS, Abboud FM, Mark AL, Walker JL. Preferential distribution of inhibitory cardiac receptors with vagal afferents to the inferoposterior wall of the left ventricle activated during coronary occlusion in the dog. Circulation Research 43 (4), 512–519, 1978.

Uemura K, Li M, Tsutsumi T, Yamazaki T, Kawada T, Kamiya A, Inagaki M, Sunagawa K, Sugimachi M. Efferent vagal nerve stimulation induces tissue inhibitor of metalloproteinase-1 in myocardial ischemia–reperfusion injury in rabbit. American Journal of Physiology. Heart and Circulatory Physiology 293 (4), H2254–H2261, 2007.

Vanoli E, de Ferrari GM, Stramba-Badiale M, Hull Jr SS, Foreman RD, Schwartz PJ. Vagal stimulation and prevention of sudden death in conscious dogs with a healed myocardial infarction. Circulation Research 68 (5), 1471–1481, 1991.

Yao Z, Gross GJ. Acetylcholine mimics ischemic preconditioning via a glibenclamide-sensitive mechanism in dogs. American Journal of Physiology 264 (6 Pt 2), H2221–H2225, 1993.

Metformin Prevents Progression of Heart Failure in Dogs
Role of AMP-Activated Protein Kinase

Hideyuki Sasaki, MD; Hiroshi Asanuma, MD, PhD; Masashi Fujita, MD, PhD; Hiroyuki Takahama, MD, PhD; Masakatsu Wakeno, MD, PhD; Shin Ito, MD; Akiko Ogai, BS; Masanori Asakura, MD, PhD; Jiyoong Kim, MD; Tetsuo Minamino, MD, PhD; Seiji Takashima, MD, PhD; Shoji Sanada, MD, PhD; Masaru Sugimachi, MD, PhD; Kazuo Komamura, MD, PhD; Naoki Mochizuki, MD, PhD; Masafumi Kitakaze, MD, PhD

Background—Some studies have shown that metformin activates AMP-activated protein kinase (AMPK) and has a potent cardioprotective effect against ischemia/reperfusion injury. Because AMPK also is activated in animal models of heart failure, we investigated whether metformin decreases cardiomyocyte apoptosis and attenuates the progression of heart failure in dogs.

Methods and Results—Treatment with metformin (10 μmol/L) protected cultured cardiomyocytes from cell death during exposure to H_2O_2 (50 μmol/L) via AMPK activation, as shown by the MTT assay, terminal deoxynucleotidyl transferase–mediated dUTP nick-end labeling staining, and flow cytometry. Continuous rapid ventricular pacing (230 bpm for 4 weeks) caused typical heart failure in dogs. Both left ventricular fractional shortening and left ventricular end-diastolic pressure were significantly improved in dogs treated with oral metformin at 100 $mg \cdot kg^{-1} \cdot d^{-1}$ (n=8) (18.6±1.8% and 11.8±1.1 mm Hg, respectively) compared with dogs receiving vehicle (n=8) (9.6±0.7% and 22±0.9 mm Hg, respectively). Metformin also promoted phosphorylation of both AMPK and endothelial nitric oxide synthase, increased plasma nitric oxide levels, and improved insulin resistance. As a result of these effects, metformin decreased apoptosis and improved cardiac function in failing canine hearts. Interestingly, another AMPK activator (AICAR) had effects equivalent to those of metformin, suggesting the primary role of AMPK activation in reducing apoptosis and preventing heart failure.

Conclusions—Metformin attenuated oxidative stress–induced cardiomyocyte apoptosis and prevented the progression of heart failure in dogs, along with activation of AMPK. Therefore, metformin may be a potential new therapy for heart failure. (***Circulation.*** **2009;119:2568-2577.)**

Key Words: AMP-activated protein kinase ■ heart failure ■ metformin ■ nitric oxide

Metformin is widely used as an antidiabetic drug with an insulin-sensitizing effect. A large-scale clinical trial (the UK Prospective Diabetes Study [UKPDS] 34) has shown that metformin therapy decreased the risk of cardiovascular death and the incidence of myocardial infarction associated with diabetes mellitus,[1] suggesting that this drug may be useful for patients who have both cardiovascular disease and diabetes mellitus. Eurich and colleagues[2] recently reported the results of a meta-analysis showing that metformin was the only antidiabetic agent to reduce all-cause mortality without causing any harm in patients who had heart failure and diabetes mellitus. These results suggest that a tight link exists between cardiovascular disease and diabetes mellitus and that metformin has a cardioprotective effect. Metformin is known to activate AMP-activated protein kinase (AMPK),[3–5] which is expressed in various tissues, including the myocardium, and plays a central role in the regulation of energy metabolism under stress conditions.[6] AMPK is activated by ischemia/reperfusion,[7–9] as well as in hearts with pressure overload hypertrophy[10] and subsequent heart failure.[11,12] In addition, Russell et al[9] have demonstrated that isolated hearts of AMPK-deleted mice show increased apoptosis and dysfunction after ischemia/reperfusion. Activation of AMPK by adiponectin also has been reported to protect cardiomyocytes against apoptosis and to attenuate myocardial ischemia/reperfusion injury in mice.[8] Furthermore, metformin has been reported to increase the production of nitric oxide (NO),[13–15] which is known to have various beneficial cardiovascular

Received August 23, 2007; accepted February 24, 2009.

From the Department of Cardiovascular Medicine, National Cardiovascular Center (H.S., H.A., H.T., M.W., S.I., A.O., M.A., J.K., K.K., M.K.) and Departments of Structural Analysis (H.S., H.T., M.W., S.I., N.M.) and Cardiovascular Dynamics (M.S., K.K.), Research Institute, National Cardiovascular Center, Suita, Osaka; Departments of Bioregulatory Medicine (H.S., H.T., M.W., S.I., N.M.) and Cardiovascular Medicine (M.F., T.M., S.T., S.S.), Osaka University Graduate School of Medicine, Suita, Osaka, Japan; and Department of Emergency Room Medicine, Kinki University School of Medicine, Osaka-Sayama (H.A.), Osaka, Japan.

The online-only Data Supplement is available with this article at http://circ.ahajournals.org/cgi/content/full/CIRCULATIONAHA.108.798561/DC1.

Correspondence to Masafumi Kitakaze, MD, PhD, Department of Cardiovascular Medicine, National Cardiovascular Center, 5–7–1 Fujishirodai, Suita, Osaka 565–8565, Japan. E-mail kitakaze@zf6.so-net.ne.jp

Circulation **is available at http://circ.ahajournals.org** **DOI: 10.1161/CIRCULATIONAHA.108.798561**

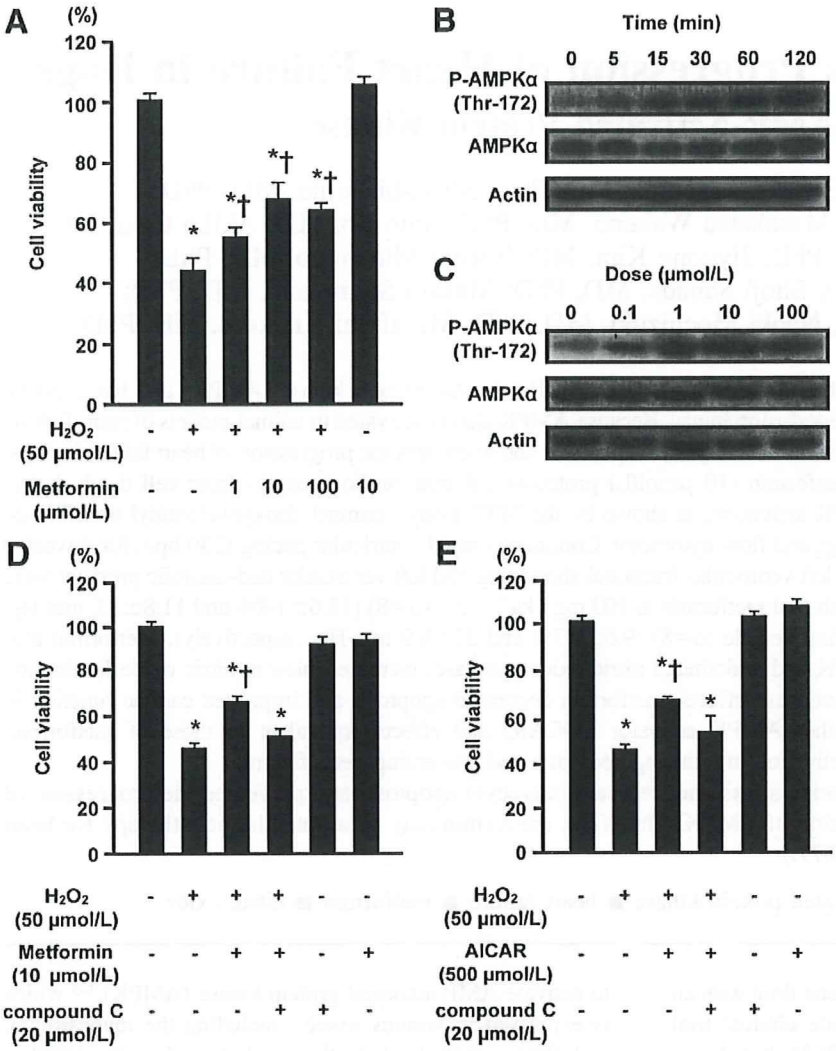

Figure 1. Effect of metformin on oxidative stress–induced cell death via AMPK activation in cultured rat cardiomyocytes. A, Cardiomyocyte viability after treatment with metformin (1, 10, or 100 μmol/L) and exposure to H_2O_2 (50 μmol/L). B, Time (0, 5, 15, 30, 60, 120 minutes) -dependent changes in AMPK phosphorylation in cardiomyocytes after treatment with metformin (10 μmol/L). C, Dose-dependent changes in AMPK phosphorylation in cardiomyocytes after treatment with metformin (0.1, 1, 10, or 100 μmol/L). D, Effect of an AMPK inhibitor (compound C; 20 μmol/L) on cardiomyocyte viability after treatment with metformin (10 μmol/L). E, Effect of an AMPK activator (AICAR; 500 μmol/L) on cardiomyocyte viability after treatment with metformin (10 μmol/L). Values are mean±SEM. P-AMPKα indicates phosphorylation of AMPKα. *$P<0.05$ vs no treatment; †$P<0.05$ vs H_2O_2 (50 μmol/L) treatment.

effects[16] and may alleviate mechanical or neurohormonal stress on the heart.

Clinical Perspective on p 2577

These findings led us to hypothesize that activation of AMPK by metformin may exert a cardioprotective effect under stress conditions. Accordingly, metformin might be a potential new treatment for cardiac failure because it activates AMPK and increases NO production. Therefore, we investigated the influence of metformin on apoptosis, an important feature of heart failure, using cultured neonatal cardiomyocytes exposed to H_2O_2 and the effect of metformin on the progression of pacing-induced heart failure in dogs, along with activation of AMPK.

Methods

Experimental procedures are described in the online-only Data Supplement.

Statistical Analysis

Results are expressed as mean±SEM. Comparison of changes between groups over time was performed by 2-way repeated-measures ANOVA. Other data were compared between groups by 1-way fractional ANOVA. The Tukey-Kramer test was used to correct for multiple comparisons. In all analyses, values of $P<0.05$ were considered to indicate statistical significance.

The authors had full access to and take full responsibility for the integrity of the data. All authors have read and agree to the manuscript as written.

Results

Metformin Attenuates Oxidative Stress–Induced Cell Death and Apoptosis in Cultured Cardiomyocytes via AMPK Activation

Cell viability was decreased in the presence of H_2O_2, as shown by the MTT assay, but this change was blunted by treatment with metformin in a dose-dependent manner (Figure 1A). Treatment with metformin (10 μmol/L) stimulated phosphorylation of AMPK in cultured cardiomyocytes in a time- and dose-dependent manner (Figure 1B and 1C). The effect of metformin on cell viability was blunted by cotreatment with compound C, an AMPK inhibitor (20 μmol/L) (Figure 1D). 5-Amino-4-imidazole-1-β-D-carboxamide ribofuranoside (AICAR; another AMPK activator) had an effect similar to metformin on cardiomyocyte viability after exposure to H_2O_2 (Figure 1E). These results suggested that

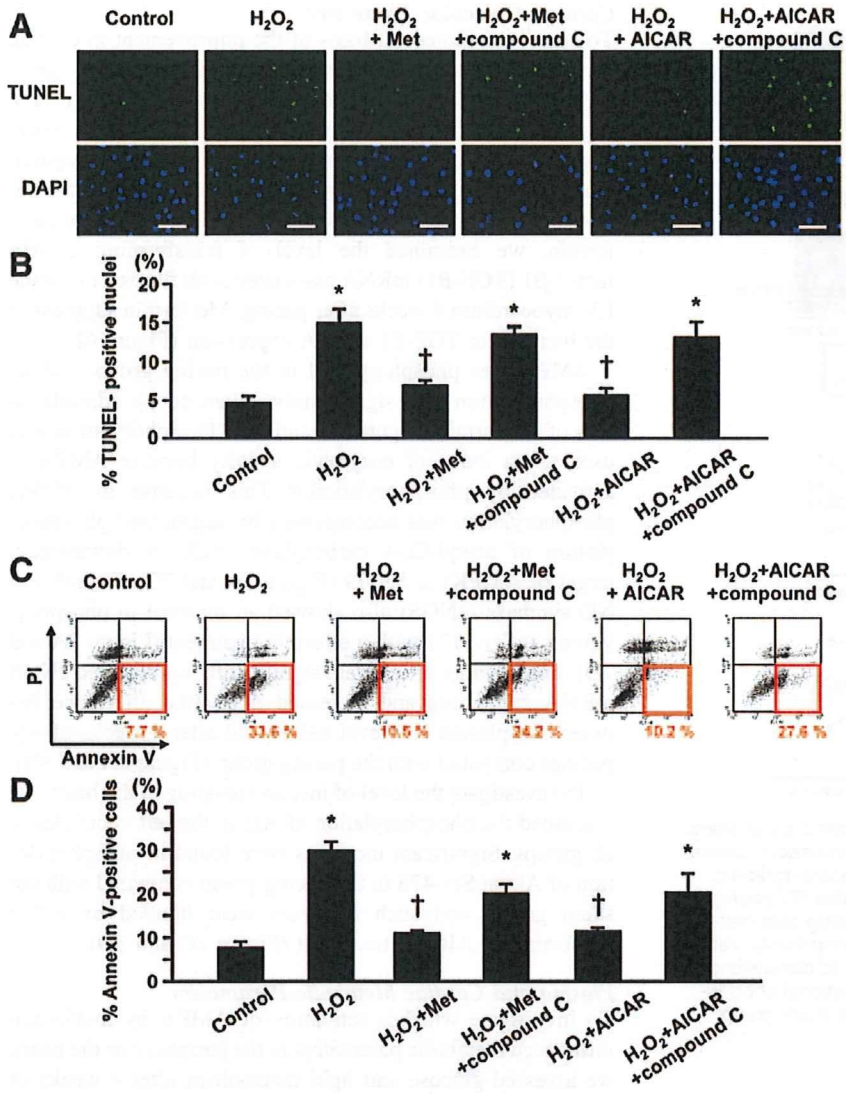

Figure 2. Effect of metformin on oxidative stress–induced apoptosis via AMPK activation in cultured rat cardiomyocytes. Representative (A) and quantitative (B) data on cardiomyocyte apoptosis obtained by TUNEL staining (n=3 in each experiment). Representative (C) and quantitative (D) data on cardiomyocyte apoptosis obtained by flow cytometry (n=3 in each experiment). Values are mean±SEM. PI indicates propidine iodide. *$P<0.05$ vs control; †$P<0.05$ vs H_2O_2 (50 μmol/L) treatment.

activation of AMPK protected cardiomyocytes against damage caused by H_2O_2.

H_2O_2 also increased cardiomyocyte apoptosis, as shown by the terminal deoxynucleotidyl transferase–mediated dUTP nick-end labeling (TUNEL) staining and flow cytometry (annexin V–positive and propidine iodide–negative cells) (Figure 2A through 2D). Metformin pretreatment significantly reduced the extent of cardiomyocyte apoptosis compared with that in untreated control cells (Figure 2A through 2D). Treatment with compound C inhibited the effects of metformin and AICAR (which was similar to that of metformin) on apoptosis in cardiomyocytes exposed to H_2O_2 (Figure 2A through 2D). These results suggested that the activation of AMPK by metformin could prevent apoptosis of cardiomyocytes induced by H_2O_2.

Effect of Metformin on Cardiac Function in Dogs With Pacing-Induced Heart Failure

Cardiac Physiological and Pathophysiological Parameters

Four weeks after the rapid right ventricular (RV) pacing, left ventricular (LV) end-diastolic dimension, LV end-systolic dimension, LV fractional shortening, and LV ejection fraction of the pacing group showed significant deterioration compared with the sham group (Figure 3A and 3B). Treatment with metformin significantly reduced both LV dimensions and increased both LV fractional shortening and LV ejection fraction compared with the pacing group (Figure 3A and 3B). Before RV pacing, both mean aortic pressure and heart rate were similar in all groups, and these parameters did not change throughout the study (Table). Four weeks after the RV pacing, pulmonary capillary wedge pressure, mean pulmonary artery pressure, and LV end-diastolic pressure were all significantly higher in the pacing group compared with the sham group (Figure 4A and 4B). Metformin treatment significantly reduced pulmonary capillary wedge pressure, mean pulmonary artery pressure, and LV end-diastolic pressure compared with the pacing group (Figure 4A and 4B). Furthermore, cardiac output was decreased and systemic vascular resistance was increased in the pacing group compared with the sham group, whereas metformin increased cardiac output and decreased systemic vascular resistance compared with the levels in the pacing group (the Table).

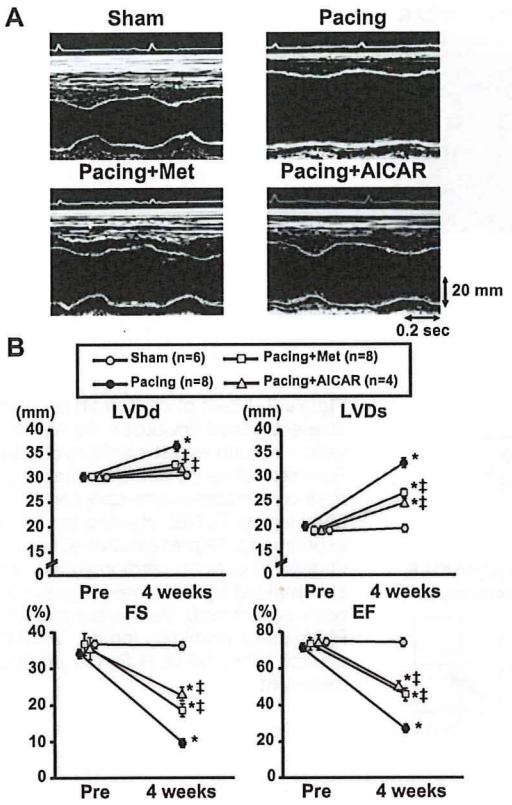

Figure 3. Effect of metformin on echocardiographic parameters. A, Representative M-mode echocardiograms obtained 4 weeks after sham surgery or after RV pacing. B, Echocardiographic parameters before and after sham surgery or after RV pacing in the sham group (n=6), pacing group (n=8), pacing plus metformin group (n=8), and pacing plus AICAR group (n=4). Values are mean±SEM. LVDd indicates LV end-diastolic dimension; LVDs, LV end-systolic dimension; LVFS, LV fractional shortening; and LVEF, LV ejection fraction. *$P<0.01$ vs sham group; ‡$P<0.01$ vs pacing group.

Importantly, the percentage of TUNEL-positive cells to total cells in LV myocardium in the pacing group increased compared with that in the sham group, which was blunted by treatment with either metformin or AICAR (Figure 5A through 5E).

Consistent with previous data,[17] no significant differences were found in body weight, the ratio of LV plus septal weight to body weight, and the ratio of RV weight to body weight among all groups (the Table).

To explore established markers of cardiac failure, we analyzed LV myocardial expression of the atrial natriuretic peptide and brain natriuretic peptide genes, which showed an increase in the pacing group, whereas metformin significantly suppressed this increase (Figure 6A and 6B). Metformin also significantly reduced the levels of angiotensin II and norepinephrine compared with the pacing group (the Table).

Pedometer counts were significantly reduced in the pacing group compared with the sham group, suggesting that heart failure led to reduced physical activities (the Table). Metformin increased the pedometer count compared with that in the pacing group. No differences in body fat were found among all groups (the Table).

Cardiac Molecular Parameters

To assess the molecular basis of the improvement in cardiac performance achieved by metformin administration for 4 weeks, we examined the collagen volume fraction in LV myocardium after staining with Masson's trichrome stain. Metformin reduced the collagen volume fraction compared with the pacing group (Figure 6C and 6D). To further investigate the mechanism of this antifibrotic effect of metformin, we examined the level of transforming growth factor-β1 (TGF-β1) mRNA associated with fibrosis in canine LV myocardium 4 weeks after pacing. Metformin suppressed the increase in TGF-β1 mRNA expression (Figure 6E).

AMPK was phosphorylated in the pacing group, and its phosphorylation was significantly enhanced by administration of metformin (Figure 7A and 7B). Phosphorylation was used as an index of enzymatic activity because AMPK is activated by phosphorylation.[18] This increase in AMPK phosphorylation was accompanied by augmented phosphorylation of acetyl-CoA carboxylase (ACC; a downstream target of AMPK) at Ser-79 (Figure 7A and 7C). Endothelial NO synthase (eNOS) also showed an increase in phosphorylation at Ser-1177 with metformin treatment (Figure 7A and 7D). Furthermore, metformin significantly upregulated eNOS mRNA expression and increased ΔNO (the difference between the plasma NO level before and after 4 weeks of RV pacing) compared with the pacing group (Figure 8A and 8B).

To investigate the level of insulin signaling in the heart, we examined the phosphorylation of Akt in the left ventricles in all groups. Significant increases were found in phosphorylation of Akt at Ser-473 in the pacing group compared with the sham group, and such increases were blunted by either metformin or AICAR treatment (Figure 8C and 8D).

Plasma and Cardiac Metabolic Parameters

To investigate whether activation of AMPK by metformin influenced metabolic parameters in the periphery or the heart, we assessed glucose and lipid metabolism after 4 weeks of pacing. Plasma free fatty acids tended to increase in the pacing group compared with the sham group, although no statistically significant difference was found. Fasting plasma levels of both glucose and lactate were similar among all groups (the Table). Both the fasting plasma insulin level and the homeostasis model assessment–insulin resistance value were significantly increased in the pacing group, whereas metformin reduced both parameters until they were similar to those of the sham group (the Table).

In the heart, both glucose extraction and the arterial–coronary sinus difference were increased in the pacing group compared with the sham group (the Table). In the pacing group, the free fatty acids extraction was not increased, but the arterial–coronary sinus difference tended to increase compared with the sham group (the Table). Lactate extraction and the arterial–coronary sinus difference were similar among all groups (the Table).

AICAR Mimics the Effect of Metformin in This Canine Pacing Model

To further confirm that activation of AMPK contributed to inhibition of the progression of heart failure, we administered

Table. Characteristics of the Dogs at 4 Weeks

	Sham Group (n=6)	Pacing Group (n=8)	Pacing+Metformin Group (n=8)	Pacing+AICAR Group (n=4)
Organ weight				
Body weight, kg	9.5±0.2	9.4±0.2	9.7±0.1	9.6±0.3
LV+septal weight, g	42±0.6	47.3±1.2	43.6±0.9	44.8±1.3
LV+septal weight/body weight ratio, g/kg	4.4±0.1	5.0±0.1	4.5±0.1	4.7±0.2
RV weight, g	14.7±0.5	15.6±0.6	15.0±1.2	14.7±1.0
RV weight/body weight ratio, g/kg	1.5±0.1	1.7±0.1	1.5±0.1	1.5±0.1
Hemodynamic parameters				
Mean aortic pressure, mm Hg	105±5	109±2	100±2	97±3.3
Heart rate, bpm	118±5	136±4	128±5	126±3.6
Cardiac output, L/min	2.6±0.1	1.6±0.1*	2.2±0.3†	2.2±0.3†
Systemic vascular resistance, dynes · s · cm^{-5}	3317±189	4769±235*	3775±334†	3763±237†
Plasma metabolic parameters				
Fasting glucose, mmol/L	5.3±0.3	5.3±0.1	5.3±0.1	5.3±0.2
Fasting insulin, μU/mL	14.2±3.3	67.6±13.7*	18.9±7.3†	24.4±10.5†
HOMA-IR	3.4±0.1	15.8±0.1*	4.4±0.1†	5.8±0.1†
Free fatty acids, μmol/L	305±67	716±68	554±101	595±69
Lactate, mmol/L	1.4±0.2	1.5±0.2	1.5±0.1	1.4±0.1
Cardiac metabolic substrates				
Glucose				
Arterial, mmol/L	5.8±0.1	6.4±0.2	6.6±0.1	6.6±0.4
Arterial–coronary sinus difference, mmol/L	0.6±0.1	1.6±0.3*	0.9±0.1	1.1±0.3
Extraction rate, %	10.5±1.2	28.6±4.7*	13.3±1.8	17.7±4.7
Free fatty acids				
Arterial, mmol/L	213.5±44.9	532.3±98.5*	312.8±56.6	294.5±22.8
Arterial–coronary sinus difference, mmol/L	90.4±13.2	153.7±20.6	99.0±9.1	103.2±20.6
Extraction rate, %	47.5±9.2	29.9±2.8	33.9±5.1	36.9±8.6
Lactate				
Arterial, mmol/L	1.8±0.1	1.9±0.3	2.3±0.7	1.8±0.8
Arterial–coronary sinus difference, mmol/L	1.2±0.3	1.0±0.2	1.3±0.5	1.1±0.4
Extraction rate, %	62.6±16.0	48.2±3.8	55.0±12.2	61.8±6.9
Plasma neurohormone levels				
Norepinephrine, pg/mL	34.9±13.0	195.9±21.3*	59.2±11.2†	79.3±8.9†
Angiotensin II, pg/mL	34.7±15.0	153.6±24.3*	78.1±14.8†	73.4±11.8†
Body fat and activity				
Body fat, %	13.7±1.2	18.7±2.9	16±1.2	14.3±0.8
Pedometer count	88 783±2899	64 541±2530*	78 423±3292†	77 716±1472†

HOMA-IR indicates homeostasis model assessment–insulin resistance. Values are mean±SEM.
*$P<0.05$ vs the sham group; †$P<0.05$ vs the pacing group.

another AMPK activator (AICAR at a dose of 5 mg/kg SC every other day) to dogs. As expected, AICAR reproduced the effects of metformin in this canine pacing model (Figures 3 through 8).

Discussion

To the best of our knowledge, this is the first study to demonstrate clearly that long-term (not short-term) oral administration of metformin, which is used as an antidiabetic agent worldwide, inhibits cardiac remodeling and prevents the progression of heart failure in dogs, along with increases in AMPK activation and NO production. Of course, we and others have previously shown that in rodent either AMPK activation or NO production attenuates myocardial ischemia/reperfusion injury in the ischemic model[7–9] and prevents cardiac remodeling in the pressure overload model.[11,12,19,20] However, it has been unclear whether AMPK or NO can modulate cardiac remodeling and inhibit the progression of heart failure in a canine model with another pathogenic mechanism that is not an ischemic or a pressure overload heart failure model. Therefore, we used a rapid pacing-induced heart failure dog model, which is considered to be similar to human dilated cardiomyopathy[21,22] and can be superimposed on translational study for human heart failure.

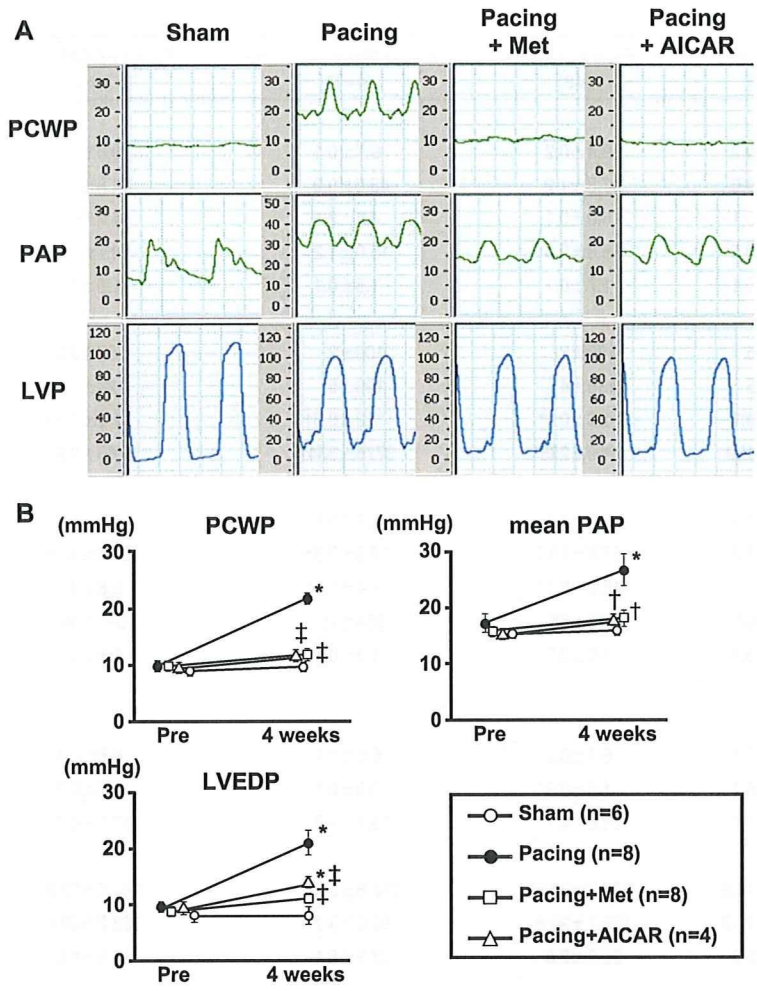

Figure 4. Effect of metformin on hemodynamic parameters. A, Representative graphs of hemodynamic parameters obtained at 4 weeks. B, Hemodynamic parameters before and after the 4-week study period in the sham (n=6), pacing (n=8), pacing plus metformin (n=8), and pacing plus AICAR (n=4) groups. Values are mean±SEM. PAP indicates pulmonary artery pressure; PCWP, pulmonary capillary wedge pressure; and LVEDP, LV end-diastolic pressure. *$P<0.05$ vs sham group; †$P<0.05$ vs pacing group; ‡$P<0.01$ vs pacing group.

Furthermore, we provide sufficient insight because dogs can be monitored more precisely for hemodynamic data than rodents.

Possible Cardioprotective Mechanism of Metformin Mediated via AMPK

Metformin has previously been shown to reduce high fat–induced apoptosis,[23] and AMPK has been reported to protect against hypoxic apoptosis in cardiomyocytes through attenuation of endoplasmic reticulum stress.[24] Consistent with these previous reports, we confirmed that metformin could ameliorate oxidative stress–induced apoptosis in cardiomyocytes. This effect was blunted by compound C, an AMPK inhibitor, suggesting that activation of AMPK was responsible for the inhibition of cardiomyocyte apoptosis. Furthermore, using a dog model, we demonstrated that metformin ameliorated the progression of heart failure induced by rapid RV pacing and decreased apoptosis in the LV myocardium, as indicated by TUNEL staining. Interestingly, AICAR, another AMPK activator, had effects almost identical to those of metformin, supporting that the activation of AMPK contributed to the observed cardioprotective effect. Indeed, AICAR also has been reported to reduce myocardial ischemia/reperfusion injury in humans and animals.[25,26] What processes following AMPK activation are involved in cardioprotection?

The first possibility is enhancement of NO production. Recchia et al[27] reported that basal cardiac NO release is decreased in dogs with heart failure induced by rapid pacing. We found that the difference in plasma NO levels between baseline and 4 weeks of RV pacing was significantly increased by metformin treatment compared with the pacing group. Metformin has been shown to phosphorylate AMPK at Thr-172 in cardiomyocytes and murine hearts,[4,5] whereas AMPK is known to phosphorylate eNOS at Ser-1177 in rat hearts,[28] resulting in an increase in NO production. Indeed, a recent report has indicated that short-term metformin treatment protects against myocardial infarction via AMPK-eNOS–mediated signaling in mice.[7] Other studies have suggested involvement of the AMPK-eNOS pathway in the response of endothelial cells to shear stress,[29] metformin,[30] and statins.[31] Consistent with these reports, we found that either metformin or AICAR promoted the phosphorylation of eNOS at Ser-1177 and increased both mRNA and protein levels of eNOS, possibly leading to increased plasma NO levels and reduced systemic vascular resistance. Although the precise mechanism of the effects of phosphorylation of AMPK by either metformin or AICAR on eNOS protein expression is not clear, these findings suggest that metformin or AICAR increased NO production, which improves endothelial

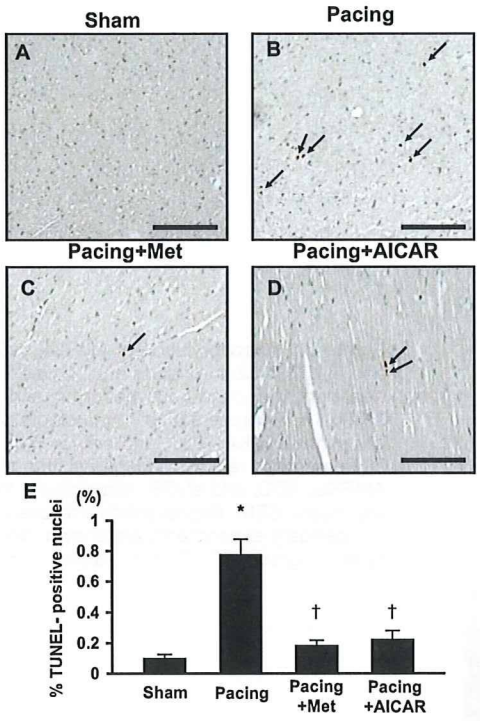

Figure 5. TUNEL staining of canine hearts at 4 weeks. Representative examples of TUNEL-stained hearts from sham (A), pacing (B), pacing plus metformin (C), and pacing plus AICAR (D) groups. Arrows indicate TUNEL-positive nuclei (brown). Scale bar=100 μm. E, Quantitative data on the percentage of TUNEL-positive nuclei to total cell nuclei. *P<0.05 vs sham group; †P<0.05 vs pacing group.

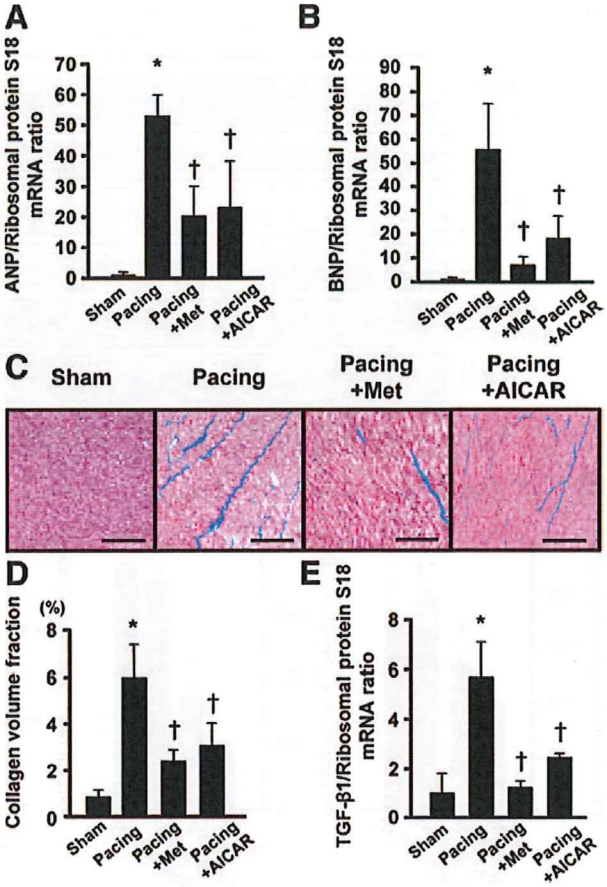

Figure 6. Natriuretic peptide expression, cardiac collagen volume fraction, and TGF-β1 expression. A, B, and E, Quantitative real-time reverse-transcriptase polymerase chain reaction analysis of myocardial atrial natriuretic peptide (ANP), brain natriuretic peptide (BNP), and TGF-β1 expression, respectively. The mRNA values were corrected for the ribosomal protein S18 mRNA level. The sham group was arbitrarily assigned a value of 1.0. Results are mean±SEM. Representative results from 3 independent experiments are shown. *P<0.05 vs sham group; #P<0.05 vs pacing group. C, Representative histological appearance of LV myocardium stained with Masson's trichrome stain (light blue). Scale bar=100 μm. D, Collagen volume fraction in the LV myocardium. Values are mean±SEM. *P<0.05 vs sham group; †P<0.05 vs pacing group.

function. NO is believed to have various cardioprotective effects.[16] Therefore, enhancement of NO production by metformin via activation of AMPK may have contributed to alleviating the progression of heart failure induced by rapid RV pacing.

The second possibility is related to the improvement in insulin resistance. It is known that insulin resistance is associated with the progression of chronic heart failure, whereas chronic heart failure may provoke insulin resistance by increasing sympathetic activity, activating the renin-angiotensin system, or both.[32,33] We found that rapid RV pacing for 4 weeks induced heart failure and that metformin treatment improved insulin resistance (estimated by homeostasis model assessment–insulin resistance) compared with the pacing group, suggesting that the beneficial effect of metformin on heart failure mediated via AMPK may have been due in part to an improvement in insulin resistance.

The third possibility is the metabolic effects of AMPK activation. Both metformin and AICAR are reported to increase glucose extraction in heart,[34,35] which may decrease the severity of the failing hearts. However, we found a 2- to 3-fold increase in myocardial glucose extraction of pacing dogs, and metformin returned glucose extraction to the value of the sham group. Numerous studies have shown a switch from free fatty acids to glucose as the primary energy substrate in humans and animals with advanced heart failure,[27,36–38] suggesting that the reduction in glucose extraction by the improvement in heart failure by AMPK activation is likely to be greater than the induction of glucose extraction by direct activation of AMPK. The possibility exists that AMPK-induced glucose extraction triggers the improvement in heart failure, followed by the restoration of metabolic switch. On the other hand, we found that the net free fatty acids extraction of the pacing group tended to increase despite no statistical significance, which is consistent with the report by Paolisso et al[39] that myocardial free fatty acids extraction increased in patients with congestive heart failure[39] but is contrary to the reports of the metabolic switch.[27,36–38] The metabolic switch may differ in relatively acute or chronic heart failure and by the severity of heart failure.

The increased phosphorylation of Akt in the pacing group was attenuated in either the pacing plus metformin or the pacing plus AICAR group, suggesting that the levels of activation of insulin signaling decreased in either the

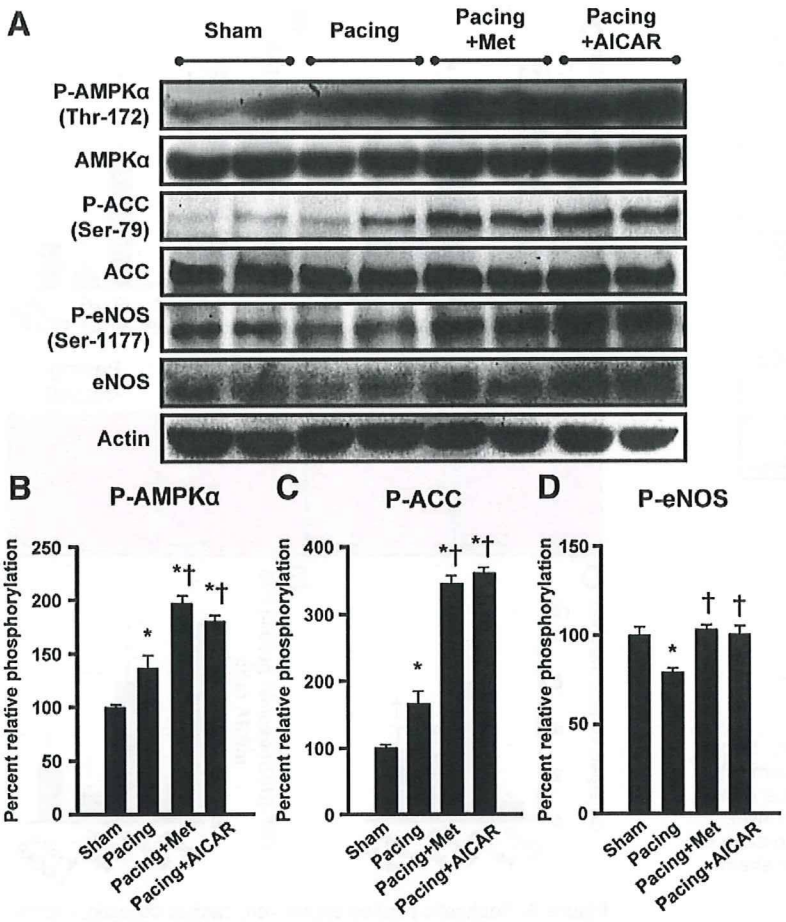

Figure 7. Phosphorylation of AMPKα, ACC, and eNOS in canine hearts after 4 weeks of treatment with or without metformin and AICAR. A, Representative immunoblots of phospho-AMPKα, ACC, and eNOS. B through D, Percentage relative phosphorylation of AMPKα, ACC, and eNOS, respectively. Values are mean±SEM. Representative results from 3 independent experiments are shown. *$P<0.05$ vs sham group; †$P<0.05$ vs pacing group.

metformin- or AICAR-treated group. Considering that glucose extraction was decreased in the pacing plus metformin and pacing plus AICAR groups and that AMPK was phosphorylated by either metformin or AICAR, which may increase in glucose extraction in the heart, the present data may be contradictory, but they are not contradictory when we consider the changes in phosphorylated Akt. The reason is that in this pacing-induced canine heart failure model, glucose extraction in the heart was influenced predominantly by insulin resistance, accompanied by the severity of heart failure, rather than AMPK phosphorylation, although further investigation on this issue is needed.

The fourth possibility is the antifibrotic effect of metformin. Several studies have indicated that AMPK activation inhibits protein synthesis through effects on both the eEF-2 and mTOR pathways.[40,41] We demonstrated that no significant difference in ventricular mass existed at autopsy among the groups. This dog pacing model has been reported to preserve wall thickness without hypertrophy or a consistent increase in heart weight, unlike the pressure overload model.[42] We found that metformin attenuated fibrosis and reduced the TGF-β1 mRNA level after 4 weeks of RV pacing compared with the pacing group. Metformin also improved representative markers of heart failure, including LV end-diastolic pressure, brain natriuretic peptide, angiotensin II, and norepinephrine. Although a number of factors may have contributed to the antifibrotic effect of metformin, our data suggest that inhibition of TGF-β1 by metformin has at least some role, resulting in the prevention of heart failure.

Taken together, these data suggest that metformin has a direct cardioprotective effect, has effects on the improvements of peripheral vascular system and insulin resistance, and inhibits fibrosis. All these actions might contribute to the improvement in the pathophysiology of heart failure, although we could not identify the exact role of each factor. It remains to be determined whether these results were a cause or consequence of improved cardiac function, especially in systemic effects of both insulin resistance and systemic vascular resistance.

Study Limitations

We found that the extent of phosphorylation of eNOS decreased despite the increase in the phosphorylated Akt in the pacing-induced failing canine hearts, which may be contradictory to previous reports that the phosphorylation of Akt leads to eNOS phosphorylation.[43,44] Because the signal transduction to modulate eNOS is unclear in the failing myocardium and the pathophysiological role and importance of Akt also are unclear, this discrepancy should be clarified in future studies.[45]

We need to consider the dose of metformin used in the present study, which was at least 3-fold higher than that used clinically. Nevertheless, adverse effects such as hypoglycemia and lactic acidosis were not detected during the experiment.

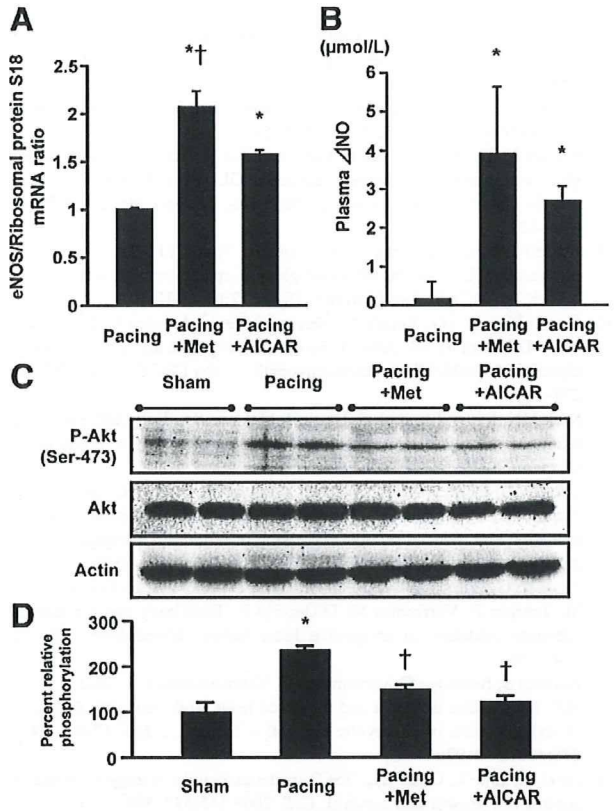

Figure 8. Effect of metformin on eNOS mRNA expression and plasma ΔNO levels, and phosphorylation of Akt in canine hearts. A, Quantitative real-time reverse-transcriptase polymerase chain reaction for eNOS mRNA. The mRNA levels were normalized to ribosomal protein S18 mRNA, and the pacing group was arbitrarily assigned a value of 1.0. B, Plasma ΔNO level after 4 weeks of RV pacing with or without metformin and AICAR administration. Values are mean±SEM. Representative results from 3 independent experiments are shown. *$P<0.05$ vs pacing group; †$P<0.05$ vs pacing plus AICAR group. C, Representative immunoblots of phospho-Akt. D, Percent relative phosphorylation of Akt. Values are mean±SEM. Representative results from 3 independent experiments are shown. *$P<0.05$ vs sham group; †$P<0.05$ vs pacing group.

Conclusions

We demonstrated that metformin prevents the progression of pacing-induced heart failure in dogs, along with the activation of AMPK. Metformin may offer a novel treatment strategy for heart failure.

Acknowledgments

We thank Yoko Horiguchi for her technical assistance; Dr Masafumi Myoishi for his assistance with TUNEL staining; Dr Hai Ying Fu for her assistance with flow cytometry; Dr Hatsue-Ishibashi-Ueda for her assistance with fluorescence microscopy; Dr Kyoko Shioya for her assistance with animal care; Tsunehisa Nakao (Nippon Shinyaku Co Ltd) for providing information about metformin; and the Evidence Finders' Club for their encouragement of this study.

Sources of Funding

This work was supported by grants in aid from the Ministry of Health, Labor, and Welfare–Japan and the Ministry of Education, Culture, Sports, Science and Technology–Japan and grants from the Japan Heart Foundation and the Japan Cardiovascular Research Foundation.

Disclosures

None.

References

1. Effect of intensive blood-glucose control with metformin on complications in overweight patients with type 2 diabetes (UKPDS 34): UK Prospective Diabetes Study (UKPDS) Group. *Lancet.* 1998;352:854–865.
2. Eurich DT, McAlister FA, Blackburn DF, Majumdar SR, Tsuyuki RT, Varney J, Johnson JA. Benefits and harms of antidiabetic agents in patients with diabetes and heart failure: systematic review. *BMJ.* 2007;335:497.
3. Zhou G, Myers R, Li Y, Chen Y, Shen X, Fenyk-Melody J, Wu M, Ventre J, Doebber T, Fujii N, Musi N, Hirshman MF, Goodyear LJ, Moller DE. Role of AMP-activated protein kinase in mechanism of metformin action. *J Clin Invest.* 2001;108:1167–1174.
4. Chan AY, Soltys CL, Young ME, Proud CG, Dyck JR. Activation of AMP-activated protein kinase inhibits protein synthesis associated with hypertrophy in the cardiac myocyte. *J Biol Chem.* 2004;279:32771–32779.
5. Zou MH, Kirkpatrick SS, Davis BJ, Nelson JS, Wiles WG 4th, Schlattner U, Neumann D, Brownlee M, Freeman MB, Goldman MH. Activation of the AMP-activated protein kinase by the anti-diabetic drug metformin in vivo: role of mitochondrial reactive nitrogen species. *J Biol Chem.* 2004;279:43940–43951.
6. Hardie DG. AMP-activated protein kinase: the guardian of cardiac energy status. *J Clin Invest.* 2004;114:465–468.
7. Calvert JW, Gundewar S, Jha S, Greer JJ, Bestermann WH, Tian R, Lefer DJ. Acute metformin therapy confers cardioprotection against myocardial infarction via AMPK-eNOS-mediated signaling. *Diabetes.* 2008;57:696–705.
8. Shibata R, Sato K, Pimentel DR, Takemura Y, Kihara S, Ohashi K, Funahashi T, Ouchi N, Walsh K. Adiponectin protects against myocardial ischemia-reperfusion injury through AMPK- and COX-2-dependent mechanisms. *Nat Med.* 2005;11:1096–1103.
9. Russell RR 3rd, Li J, Coven DL, Pypaert M, Zechner C, Palmeri M, Giordano FJ, Mu J, Birnbaum MJ, Young LH. AMP-activated protein kinase mediates ischemic glucose uptake and prevents postischemic cardiac dysfunction, apoptosis, and injury. *J Clin Invest.* 2004;114:495–503.
10. Tian R, Musi N, D'Agostino J, Hirshman MF, Goodyear LJ. Increased adenosine monophosphate-activated protein kinase activity in rat hearts with pressure-overload hypertrophy. *Circulation.* 2001;104:1664–1669.
11. Shibata R, Ouchi N, Ito M, Kihara S, Shiojima I, Pimentel DR, Kumada M, Sato K, Schiekofer S, Ohashi K, Funahashi T, Colucci WS, Walsh K. Adiponectin-mediated modulation of hypertrophic signals in the heart. *Nat Med.* 2004;10:1384–1389.
12. Liao Y, Takashima S, Maeda N, Ouchi N, Komamura K, Shimomura I, Hori M, Matsuzawa Y, Funahashi T, Kitakaze M. Exacerbation of heart failure in adiponectin-deficient mice due to impaired regulation of AMPK and glucose metabolism. *Cardiovasc Res.* 2005;67:705–713.
13. Bhalla RC, Toth KF, Tan E, Bhatty RA, Mathias E, Sharma RV. Vascular effects of metformin: possible mechanisms for its antihypertensive action in the spontaneously hypertensive rat. *Am J Hypertens.* 1996;9:570–576.
14. Marfella R, Acampora R, Verrazzo G, Ziccardi P, De Rosa N, Giunta R, Giugliano D. Metformin improves hemodynamic and rheological responses to L-arginine in NIDDM patients. *Diabetes Care.* 1996;19:934–939.
15. Katakam PV, Ujhelyi MR, Hoenig M, Miller AW. Metformin improves vascular function in insulin-resistant rats. *Hypertension.* 2000;35:108–112.
16. Rakhit RD, Marber MS. Nitric oxide: an emerging role in cardioprotection? *Heart.* 2001;86:368–372.
17. Komamura K, Shannon RP, Pasipoularides A, Ihara T, Lader AS, Patrick TA, Bishop SP, Vatner SF. Alterations in left ventricular diastolic function in conscious dogs with pacing-induced heart failure. *J Clin Invest.* 1992;89:1825–1838.
18. Lei B, Matsuo K, Labinskyy V, Sharma N, Chandler MP, Ahn A, Hintze TH, Stanley WC, Recchia FA. Exogenous nitric oxide reduces glucose transporters translocation and lactate production in ischemic myocardium in vivo. *Proc Natl Acad Sci U S A.* 2005;102:6966–6971.
19. Li HL, Yin R, Chen D, Liu D, Wang D, Yang Q, Dong YG. Long-term activation of adenosine monophosphate-activated protein kinase

attenuates pressure-overload-induced cardiac hypertrophy. *J Cell Biochem.* 2007;100:1086–1099.
20. Liao Y, Asakura M, Takashima S, Ogai A, Asano Y, Shintani Y, Minamino T, Asanuma H, Sanada S, Kim J, Kitamura S, Tomoike H, Hori M, Kitakaze M. Celiprolol, a vasodilatory beta-blocker, inhibits pressure overload-induced cardiac hypertrophy and prevents the transition to heart failure via nitric oxide-dependent mechanisms in mice. *Circulation.* 2004;110:692–699.
21. Elsner D, Riegger GA. Characteristics and clinical relevance of animal models of heart failure. *Curr Opin Cardiol.* 1995;10:253–259.
22. Lee WL, Chen JW, Ting CT, Ishiwata T, Lin SJ, Korc M, Wang PH. Insulin-like growth factor I improves cardiovascular function and suppresses apoptosis of cardiomyocytes in dilated cardiomyopathy. *Endocrinology.* 1999;140:4831–4840.
23. An D, Kewalramani G, Chan JK, Qi D, Ghosh S, Pulinilkunnil T, Abrahani A, Innis SM, Rodrigues B. Metformin influences cardiomyocyte cell death by pathways that are dependent and independent of caspase-3. *Diabetologia.* 2006;49:2174–2184.
24. Terai K, Hiramoto Y, Masaki M, Sugiyama S, Kuroda T, Hori M, Kawase I, Hirota H. AMP-activated protein kinase protects cardiomyocytes against hypoxic injury through attenuation of endoplasmic reticulum stress. *Mol Cell Biol.* 2005;25:9554–9575.
25. Mangano DT. Effects of acadesine on myocardial infarction, stroke, and death following surgery: a meta-analysis of the 5 international randomized trials: the Multicenter Study of Perioperative Ischemia (McSPI) Research Group. *JAMA.* 1997;277:325–332.
26. Kitakaze M, Takashima S, Minamino T, Node K, Shinozaki Y, Mori H, Kuzuya T, Hori M. Improvement by 5-amino-4-imidazole carboxamide riboside of the contractile dysfunction that follows brief periods of ischemia through increases in ecto-5-nucleotidase activity and adenosine release in canine hearts. *Jpn Circ J.* 1999;63:542–553.
27. Recchia FA, McConnell PI, Bernstein RD, Vogel TR, Xu X, Hintze TH. Reduced nitric oxide production and altered myocardial metabolism during the decompensation of pacing-induced heart failure in the conscious dog. *Circ Res.* 1998;83:969–979.
28. Chen ZP, Mitchelhill KI, Michell BJ, Stapleton D, Rodriguez-Crespo I, Witters LA, Power DA, Ortiz de Montellano PR, Kemp BE. AMP-activated protein kinase phosphorylation of endothelial NO synthase. *FEBS Lett.* 1999;443:285–289.
29. Zhang Y, Lee TS, Kolb EM, Sun K, Lu X, Sladek FM, Kassab GS, Garland T Jr, Shyy JY. AMP-activated protein kinase is involved in endothelial NO synthase activation in response to shear stress. *Arterioscler Thromb Vasc Biol.* 2006;26:1281–1287.
30. Davis BJ, Xie Z, Viollet B, Zou MH. Activation of the AMP-activated kinase by antidiabetes drug metformin stimulates nitric oxide synthesis in vivo by promoting the association of heat shock protein 90 and endothelial nitric oxide synthase. *Diabetes.* 2006;55:496–505.
31. Sun W, Lee TS, Zhu M, Gu C, Wang Y, Zhu Y, Shyy JY. Statins activate AMP-activated protein kinase in vitro and in vivo. *Circulation.* 2006; 114:2655–2662.
32. Swan JW, Anker SD, Walton C, Godsland IF, Clark AL, Leyva F, Stevenson JC, Coats AJ. Insulin resistance in chronic heart failure: relation to severity and etiology of heart failure. *J Am Coll Cardiol.* 1997;30:527–532.
33. Nielson C, Lange T. Blood glucose and heart failure in nondiabetic patients. *Diabetes Care.* 2005;28:607–611.
34. Fischer Y, Thomas J, Rosen P, Kammermeier H. Action of metformin on glucose transport and glucose transporter GLUT1 and GLUT4 in heart muscle cells from healthy and diabetic rats. *Endocrinology.* 1995;136: 412–420.
35. Russell RR 3rd, Bergeron R, Shulman GI, Young LH. Translocation of myocardial GLUT-4 and increased glucose uptake through activation of AMPK by AICAR. *Am J Physiol.* 1999;277:H643–H649.
36. Davila-Roman VG, Vedala G, Herrero P, de las Fuentes L, Rogers JG, Kelly DP, Gropler RJ. Altered myocardial fatty acid and glucose metabolism in idiopathic dilated cardiomyopathy. *J Am Coll Cardiol.* 2002;40: 271–277.
37. Sack MN, Rader TA, Park S, Bastin J, McCune SA, Kelly DP. Fatty acid oxidation enzyme gene expression is downregulated in the failing heart. *Circulation.* 1996;94:2837–2842.
38. Osorio JC, Stanley WC, Linke A, Castellari M, Diep QN, Panchal AR, Hintze TH, Lopaschuk GD, Recchia FA. Impaired myocardial fatty acid oxidation and reduced protein expression of retinoid X receptor-alpha in pacing-induced heart failure. *Circulation.* 2002;106:606–612.
39. Paolisso G, Gambardella A, Galzerano D, D'Amore A, Rubino P, Verza M, Teasuro P, Varricchio M, D'Onofrio F. Total-body and myocardial substrate oxidation in congestive heart failure. *Metabolism.* 1994;43: 174–179.
40. Horman S, Beauloye C, Vertommen D, Vanoverschelde JL, Hue L, Rider MH. Myocardial ischemia and increased heart work modulate the phosphorylation state of eukaryotic elongation factor-2. *J Biol Chem.* 2003; 278:41970–41976.
41. Inoki K, Zhu T, Guan KL. TSC2 mediates cellular energy response to control cell growth and survival. *Cell.* 2003;115:577–590.
42. Shinbane JS, Wood MA, Jensen DN, Ellenbogen KA, Fitzpatrick AP, Scheinman MM. Tachycardia-induced cardiomyopathy: a review of animal models and clinical studies. *J Am Coll Cardiol.* 1997;29: 709–715.
43. Montagnani M, Chen H, Barr VA, Quon MJ. Insulin-stimulated activation of eNOS is independent of Ca^{2+} but requires phosphorylation by Akt at Ser(1179). *J Biol Chem.* 2001;276:30392–30398.
44. Fulton D, Gratton JP, McCabe TJ, Fontana J, Fujio Y, Walsh K, Franke TF, Papapetropoulos A, Sessa WC. Regulation of endothelium-derived nitric oxide production by the protein kinase Akt. *Nature.* 1999;399: 597–601.
45. Shiojima I, Walsh K. Regulation of cardiac growth and coronary angiogenesis by the Akt/PKB signaling pathway. *Genes Dev.* 2006;20: 3347–3365.

CLINICAL PERSPECTIVE

Metformin is widely used as an antidiabetic drug with an insulin-sensitizing effect. A large-scale clinical trial (the UK Prospective Diabetes Study [UKPDS] 34) has shown that metformin therapy decreased the risk of cardiovascular death and the incidence of myocardial infarction associated with diabetes mellitus; metformin reduced the hemoglobin A_{1c} levels in treated patients to the same extent as in the other patients treated with conventional therapies. These results suggest that metformin might exert cardioprotective effects beyond its glucose-lowering action such as either activation of AMP-activated protein kinase (AMPK) or elevation of nitric oxide. Metformin is known to activate AMPK, which mediates potent cardioprotection against ischemia/reperfusion injury. AMPK also is activated in experimental failing myocardium, suggesting that activation of AMPK is beneficial for the pathophysiology of heart failure. The present study demonstrated that long-term oral administration of metformin prevents the progression of heart failure as indicated by hemodynamic and echocardiographic parameters. Metformin also promoted phosphorylation of both AMPK and endothelial nitric oxide synthase, increased plasma nitric oxide levels, and improved insulin resistance. As a result of these effects, metformin decreased apoptosis and improved cardiac function in failing canine hearts. Interestingly, another AMPK activator (AICAR) had effects equivalent to those of metformin, suggesting the primary role of AMPK activation in reducing apoptosis and preventing heart failure. Drugs that activate AMPK, especially metformin, may provide a novel strategy for the treatment of heart failure in clinical settings.

Autonomic Neuroscience: Basic and Clinical 148 (2009) 44–49

Contents lists available at ScienceDirect

Autonomic Neuroscience: Basic and Clinical

journal homepage: www.elsevier.com/locate/autneu

In vivo direct monitoring of vagal acetylcholine release to the sinoatrial node

Shuji Shimizu [a,c,d,*], Tsuyoshi Akiyama [b], Toru Kawada [a], Toshiaki Shishido [a], Toji Yamazaki [b], Atsunori Kamiya [a], Masaki Mizuno [a], Shunji Sano [c], Masaru Sugimachi [a]

[a] Department of Cardiovascular Dynamics, Advanced Medical Engineering Center, National Cardiovascular Center Research Institute, Osaka, Japan
[b] Department of Cardiac Physiology, National Cardiovascular Center Research Institute, Osaka, Japan
[c] Department of Cardiovascular Surgery, Okayama University Graduate School of Medicine, Dentistry and Pharmaceutical Sciences, Okayama, Japan
[d] Japan Association for the Advancement of Medical Equipment, Tokyo, Japan

ARTICLE INFO

Article history:
Received 30 September 2008
Received in revised form 16 February 2009
Accepted 23 February 2009

Keywords:
Heart rate
Vagal nerve activity
Acetylcholine
Sinoatrial node
Right atrium
Microdialysis
Anesthetized rabbit

ABSTRACT

To directly monitor vagal acetylcholine (ACh) release into the sinoatrial node, which regulates heart rate, we implanted a microdialysis probe in the right atrium near the sinoatrial node and in the right ventricle of anesthetized rabbits, and perfused with Ringer's solution containing eserine. (1) Electrical stimulation of right or left cervical vagal nerve decreased atrial rate and increased dialysate ACh concentration in the right atrium in a frequency-dependent manner. Compared to left vagal stimulation, right vagal nerve stimulation decreased atrial rate to a greater extent at all frequencies, and increased dialysate ACh concentration to a greater extent at 10 and 20 Hz. However, dialysate ACh concentration in the right atrium correlated well with atrial rate independent of whether electrical stimulation was applied to the right or left vagal nerve (atrial rate $= 304 - 131 \times \log[\mathrm{ACh}]$, $R^2 = 0.77$). (2) Right or left vagal nerve stimulation at 20 Hz decreased atrial rate and increased dialysate ACh concentrations in both the right atrium (right, 17.9 ± 4.0 nM; left, 7.9 ± 1.4 nM) and right ventricle (right, 0.9 ± 0.3 nM; left, 1.0 ± 0.4 nM). However, atrial dialysate ACh concentrations were significantly higher than ventricular concentrations, while ventricular dialysate ACh concentrations were not significantly different between right and left vagal nerve stimulation. (3) The response of ACh release to right and left vagal nerve stimulation was abolished by intravenous administration of a ganglionic blocker, hexamethonium bromide. In conclusion, ACh concentration in dialysate from the right atrium, sampled by microdialysis, is a good marker of ACh release from postganglionic vagal nerves to the sinoatrial node.

1. Introduction

Parasympathetic nerves play an important role in the regulation of heart rate under physiological conditions. To better understand the parasympathetic control of heart rate, it is important to quantitatively assess the efferent cardiac vagal nerve activity. Several methods have been used to assess this activity. Efferent cardiac vagal nerve electrical activity has been measured directly at the preganglionic site in several studies (Jewett, 1964; Kunze, 1972). We have developed a microdialysis technique which is used with high-performance liquid chromatography (HPLC) to monitor in vivo endogenous acetylcholine (ACh) release in the heart (Akiyama et al., 1994). Using this technique, we were able to monitor endogenous ACh release into the ventricular myocardium (Akiyama et al., 1994; Kawada et al., 2001). This technique permits the estimation of relative changes in postganglionic efferent cardiac vagal nerve activity in the ventricle.

However, vagal innervation is known to be heterogeneous in the heart. Kilbinger and Löffelholz (1976) reported that the ACh content of the ventricle was 41% and 19% of the atrial content in chicken and rabbit, respectively. Brown (1976) reported that ACh concentration was higher in the atrium than the ventricle, and that ACh content was higher in the right than the left portions in both the atrium and ventricle of the cat. Thus, to better understand the parasympathetic control of heart rate, which is the sinus rate under physiological conditions, we need information about the activities of postganglionic vagal nerves innervating the sinoatrial (SA) node.

In this study, we developed a dialysis probe using shorter dialysis fiber, which was suitable for implantation into the atrium. Using this dialysis probe, we tried to monitor myocardial interstitial ACh levels in the right atrium, especially near the SA node. Furthermore, we investigated whether the myocardial interstitial ACh levels reflect relative changes in activity of postganglionic vagal nerves innervating the SA node.

2. Materials and methods

2.1. Surgical preparation

Animal care was provided in accordance with the *Guiding Principles for the Care and Use of Animals in the Field of Physiological Sciences*

* Corresponding author. Department of Cardiovascular Dynamics, Advanced Medical Engineering Center, National Cardiovascular Center Research Institute, 5-7-1, Fujishiro-dai, Suita, Osaka, 565-8565 Japan. Tel.: +81 6 6833 5012; fax: +81 6 6835 5403.
E-mail address: shujismz@ri.ncvc.go.jp (S. Shimizu).

1566-0702/$ – see front matter © 2009 Elsevier B.V. All rights reserved.
doi:10.1016/j.autneu.2009.02.006

approved by the Physiological Society of Japan. All protocols were approved by the Animal Subject Committee of the National Cardiovascular Center. Forty-three Japanese white rabbits weighing from 2.2 to 2.9 kg were anesthetized using an intravenous injection of pentobarbital sodium (50 mg/kg) via the marginal ear vein, followed by a continuous intravenous infusion of α-chloralose and urethane (16 mg/kg/h and 100 mg/kg/h) through a catheter inserted into the femoral vein to maintain an appropriate level of anesthesia. The animals were intubated and ventilated mechanically with room air mixed with oxygen. Systemic arterial pressure was monitored by a catheter inserted into the femoral artery. Esophageal temperature, which was measured by a thermometer (CTM-303, TERUMO, Japan), was maintained between 38 and 39 °C using a heating pad. In all protocols, bilateral vagal nerves were exposed through a midline cervical incision and sectioned at the neck after the control dialysate sampling. A pair of bipolar stainless steel electrodes was attached to the efferent side of the right or left vagal nerve. The nerve and electrode were covered with warmed mineral oil for insulation. When vagal stimulation was required, the efferent vagal nerve was stimulated by a digital stimulator (SEN-7203, Nihon Kohden, Japan). The pulse duration and amplitude of nerve stimulation were set at 1 ms and 10 V.

With the animal in the lateral position, right lateral thoracotomy was performed and the right 3rd to 5th ribs were partially resected to expose the heart. After incision of the pericardium, stainless steel wires were attached to the apex and the anterior wall of the left ventricle for ventricular pacing. To prevent severe bradycardia and cardiac arrest induced by vagal stimulation, left ventricular pacing was performed at the same frequency as the heart rate before vagal stimulation. The ventricular rate was determined from the electrocardiogram using a cardiotachometer. Another pair of stainless steel wires was attached to the appendage of the right atrium for recording atrial electrocardiogram, from which atrial rate was determined. Heparin sodium (100 IU/kg) was administered intravenously to prevent blood coagulation. At the end of the experiment, animals were killed with an overdose injection of pentobarbital sodium. A postmortem examination confirmed that the dialysate probe did not penetrate into the atrial or ventricular cavity and the dialysis membrane was positioned totally within the atrial or ventricular wall.

2.2. Dialysis technique

The materials and properties of the dialysis probe have been described previously (Akiyama et al., 1994). Briefly, we designed a handmade transverse dialysis probe. A dialysis fiber of semipermeable membrane (4 mm length, 310 μm outer diameter, 200 μm inner diameter; PAN-1200, 50,000 molecular weight cutoff; Asahi Chemical, Tokyo, Japan) was attached at both ends to polyethylene tubes (25 cm length, 500 μm outer diameter, 200 μm inner diameter). A fine guiding needle (30 mm length, 510 μm outer diameter, 250 μm inner diameter) with a stainless steel rod (5 mm length, 250 μm outer diameter) was used for the implantation of the dialysis probe. In protocol 1 and 3, a dialysis probe was implanted in the right atrium near the junction between the superior vena cava and the right atrium. In protocol 2, a dialysis probe was also implanted in the right ventricular free wall. After implantation, the dialysis probe was perfused with Ringer's solution (NaCl 147 mM, KCl 4 mM, $CaCl_2$ 3 mM) containing the cholinesterase inhibitor eserine (100 μM) at a speed of 2 μl/min, using a microinjection pump (CMA/100, Carnegie Medicin, Sweden). Experimental protocols were started 120 min after implantation of the dialysis probe. We took account of the dead space between the dialysis membrane and the sample tube at the start of each dialysate sampling. Phosphate buffer (4 μl) containing an internal standard (isopropylhomocholine chloride) was transferred into each sample tube before dialysate sampling. Dialysate sampling periods were set at 10 min (1 sample volume = 20 μl).

2.3. Analytic procedure

Dialysate ACh was assayed using HPLC with electrochemical detection. An autosampler (CMA/200, Carnegie Medicin) was used. The HPLC system consisted of a pump with a pulse dumper (EP-300, Eicom, Japan), a separation column (AC-Gel, styrene polymer, 4 μm particle size, 2 mm inner diameter × 150 mm length, Eicom), an immobilized enzyme column (AC-Enzymepack, 1 mm inner diameter × 4 mm length, Eicom), an electrochemical detector (ECD-300, Eicom), and a degasser (DG-300, Eicom). The electrochemical detector was operated with a platinum working electrode at + 0.45 V vs. an Ag/AgCl reference electrode. The mobile phase was 50 mM potassium bicarbonate solution containing 400 mg/L of sodium 1-decansulfonate and 50 mg/L of disodium–EDTA. The pump flow rate was 0.15 ml/min.

Chromatograms were recorded and analyzed by an analog-to-digital converter (Power Chrom EPC-300, AD Instruments, Australia) with a computer. Concentrations of ACh and isopropylhomocholine chloride were determined by measuring the peak areas. The absolute detection limit of ACh was 10 fmol/injection (signal-to-noise ratio = 3).

2.4. Experimental protocols

2.4.1. Protocol 1

To examine whether atrial dialysate ACh concentration reflects ACh release from cardiac vagal nerves, we investigated the relationship between the dialysate ACh concentration in the right atrium and the frequency of right and left vagal nerve stimulation. We sampled control dialysate before and after vagal transection. Then we stimulated the right ($n = 8$) or left ($n = 8$) efferent vagal nerves for 10 min at frequencies of 5, 10, 20 and 40 Hz, and sampled dialysate during each stimulation. Ten minutes after vagal nerve stimulation, we sampled the dialysate again to check the recovery of ACh levels.

2.4.2. Protocol 2

To investigate the difference in vagal innervation density between the right atrium and right ventricle, we compared the atrial and ventricular dialysate ACh concentrations under control condition and during electrical vagal nerve stimulation. Control dialysates were sampled after vagal transection. Then the right ($n = 5$) or left ($n = 5$) efferent vagal nerve was stimulated for 10 min at a frequency of 20 Hz, and dialysates were collected during vagal stimulation.

2.4.3. Protocol 3

ACh is released from both pre- and post-ganglionic vagal nerves as a primary neurotransmitter. The cardiac vagal nerve ganglia are localized near the atrium (Löffelholz and Pappano, 1985). Electrical stimulation of cervical vagal nerves activates the entire efferent parasympathetic pathway, including both preganglionic and postganglionic nerves in the atrium. Thus it is possible that pre- and/or post-ganglionic nerves serve as the source of dialysate ACh. To determine whether pre- or post-ganglionic nerves are the source of atrial dialysate ACh, we observed ACh release in response to nerve stimulation before and after blockade of ganglionic transmission. We sampled control dialysate after vagal transection. Then we stimulated the right ($n = 9$) or left ($n = 8$) vagal nerve at a frequency of 20 Hz before and after intravenous administration of hexamethonium bromide (30 mg/kg) and sampled dialysate during vagal stimulation. To prevent severe hypotension induced by hexamethonium, arterial pressure was maintained by continuous intravenous infusion of phenylephrine (17.2 ± 1.6 μg/kg/min).

2.5. Statistical analysis

All data are presented as mean ± SE. For each protocol, heart rate and mean arterial pressure were compared by one-way repeated measures analysis of variance followed by a Dunnett's test against

control (Glantz, 2005). In protocol 1, we compared vagal stimulation-induced ACh release among the seven groups by one-way repeated measures analysis of variance followed by Tukey's test. Heart rates (atrial rate) and dialysate ACh concentrations during right and left vagal stimulation were compared by unpaired *t*-test. After logarithmic transformation of atrial dialysate ACh concentration, a linear regression analysis was performed to examine the relation between dialysate ACh concentration and atrial rate. In protocol 2, we compared atrial and ventricular dialysate ACh concentrations during vagal stimulation by two-way repeated measures analysis of variance. We also compared the effects of right and left vagal stimulation on atrial and ventricular dialysate ACh concentrations using an unpaired *t*-test. In protocol 3, we compared stimulation-induced ACh release with and without hexamethonium using one-way repeated measures analysis of variance followed by a Dunnett's test against control. Differences were considered significant at $P<0.05$.

3. Results

3.1. Protocol 1

Responses of heart rate and mean arterial pressure to electrical vagal nerve stimulation are shown in Table 1. Transection of bilateral vagal nerves did not change heart rate or mean arterial pressure significantly. While both right and left vagal stimulation decreased heart rate in proportion to the frequency of the stimulus, right vagal nerve stimulation decreased the heart rate to a greater extent than left vagal nerve stimulation at all stimulus frequencies tested ($P<0.05$ at 5 Hz, $P<0.01$ at 10 Hz, $P<0.05$ at 20 Hz and $P<0.05$ at 40 Hz). Heart rate recovered to the pre-stimulation levels after stimulation. Both right and left vagal nerve stimulation with ventricular pacing decreased mean arterial pressure. Mean arterial pressure recovered partially but remained lower than the pre-stimulation levels 10 min after stimulation.

Transection of bilateral vagal nerves did not change dialysate ACh concentration (Fig. 1). Both right and left vagal stimulation increased the dialysate ACh concentration in proportion to the stimulus frequency. Right vagal stimulation increased the dialysate ACh concentration from 1.9±0.3 nM in the post-transection control to 2.7±0.4 nM at 5 Hz ($P<0.05$ vs. control), 5.5±0.8 nM at 10 Hz ($P<0.01$ vs. 5 Hz), 17.2±3.0 nM at 20 Hz ($P<0.01$ vs. 10 Hz) and 40.4±8.4 nM at 40 Hz ($P<0.01$ vs. 20 Hz). Dialysate ACh concentration recovered to 2.2±0.3 nM 10 min after stimulation. Left vagal stimulation increased dialysate ACh concentration from 1.6±0.3 nM in the post-transection control to 2.2±0.4 nM at 5 Hz (N.S. vs. control), 3.2±0.5 nM at 10 Hz ($P<0.01$ vs. control), 8.2±1.4 nM at 20 Hz ($P<0.01$ vs. 10 Hz) and 24.7±4.6 nM at 40 Hz ($P<0.01$ vs. 20 Hz). Dialysate ACh concentration recovered to 2.0±0.5 nM 10 min after stimulation. While both right and left vagal stimulation increased dialysate ACh concentration in a frequency-dependent manner, right vagal nerve stimulation increased dialysate ACh concentration to a greater extent than left vagal nerve stimulation at 10 and 20 Hz (N.S. at 5 Hz, $P<0.05$ at 10 Hz, $P<0.05$ at 20 Hz and N.S. at 40 Hz).

Table 1
Responses of heart rate and mean arterial pressure to electrical vagal nerve stimulation (protocol 1).

	Heart rate (bpm)	Mean arterial pressure (mm Hg)
Rt vagal stimulation ($n=8$)	Atrial rate (pacing rate)	
Control before transection	298±8	83±4
Control after transection	293±7	85±6
VNS (5 Hz)	246±5** (296±5)	71±7
VNS (10 Hz)	201±6** (296±5)	77±6
VNS (20 Hz)	121±7** (296±5)	72±8
VNS (40 Hz)	88±4** (296±5)	65±7**
After VNS	287±10	70±9
Lt vagal stimulation ($n=8$)	Atrial rate (pacing rate)	
Control before transection	305±8	89±4
Control after transection	308±5	92±6
VNS (5 Hz)	267±6* (309±4)	79±6**
VNS (10 Hz)	236±10** (309±4)	82±6
VNS (20 Hz)	165±13** (309±4)	77±5**
VNS (40 Hz)	129±16** (309±4)	67±6**
After VNS	305±13	75±8**

Values are means±SE; *n*: numbers of rabbits; Rt: right; Lt: left; VNS: electrical vagal nerve stimulation; **$P<0.01$ vs. control; *$P<0.05$ vs. control.

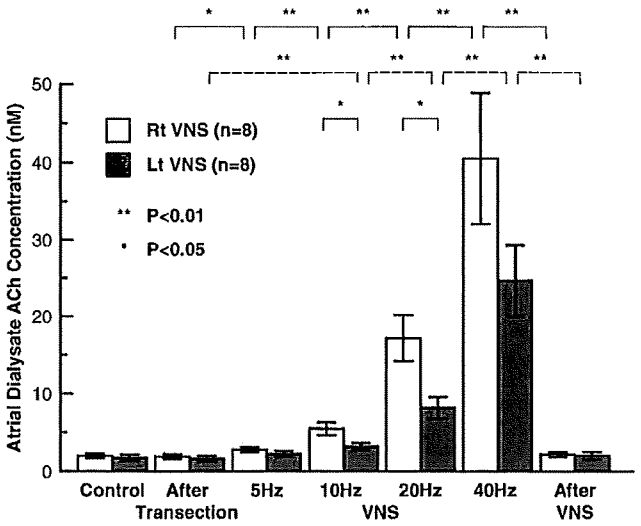

Fig. 1. Dialysate ACh concentrations of controls and during electrical vagal nerve stimulation at different frequencies. Right vagal nerve stimulation increased atrial dialysate ACh concentration from 1.9±0.3 nM in the post-transection control to 2.7±0.4 nM at 5 Hz, 5.5±0.8 nM at 10 Hz, 17.2±3.0 nM at 20 Hz and 40.4±8.4 nM at 40 Hz. Left vagal nerve stimulation increased atrial dialysate ACh concentration from 1.6±0.3 nM in the control to 2.2±0.4 nM at 5 Hz, 3.2±0.5 nM at 10 Hz, 8.2±1.4 nM at 20 Hz and 24.7±4.6 nM at 40 Hz. Values are means±SE; Rt: right; Lt: left; VNS: electrical vagal nerve stimulation; *n*: number of rabbits: **$P<0.01$, *$P<0.05$.

The relationship between dialysate ACh concentration and atrial rate ($n=16$) is shown in Fig. 2. Dialysate ACh concentration in the right atrium correlated well with atrial rate (AR; $AR=304-131\times\log[ACh]$, $R^2=0.77$). There was no significant difference in the intercept or slope of regression line between right and left vagal nerve stimulation (right: $AR=304-135\times\log[ACh]$, $R^2=0.79$; left: $AR=303-126\times\log[ACh]$, $R^2=0.73$) (Glantz, 2005). The correlation between dialysate ACh concentration and atrial rate was independent of the side of vagal nerve stimulation.

3.2. Protocol 2

Responses of heart rate and mean arterial pressure were similar to the responses to vagal stimulation at 20 Hz in protocol 1 (Table 2). Responses of ACh release in the right atrium and right ventricle to vagal stimulation are shown in Fig. 3. Right vagal stimulation increased the atrial dialysate ACh concentration from 2.6±0.6 nM in the post-transection control to 17.9±4.0 nM ($P<0.01$) and the ventricular dialysate ACh concentration from 0.4±0.2 nM to 0.9±0.3 nM ($P<0.01$). Left vagal stimulation also increased the atrial dialysate ACh concentration from 1.5±0.4 nM to 7.9±1.4 nM ($P<0.01$) and the ventricular dialysate ACh concentration from 0.3±0.1 nM in the control to 1.0±0.4 nM ($P<0.01$). Atrial dialysate ACh concentrations were higher than ventricular dialysate ACh concentrations in both right and left vagal stimulation ($P<0.01$). The interaction between the stimulation and the position of probe (atrium or ventricle) was significant ($P<0.01$). There was no difference in ventricular dialysate ACh concentration between right and left vagal stimulation, but atrial dialysate ACh concentration was significantly

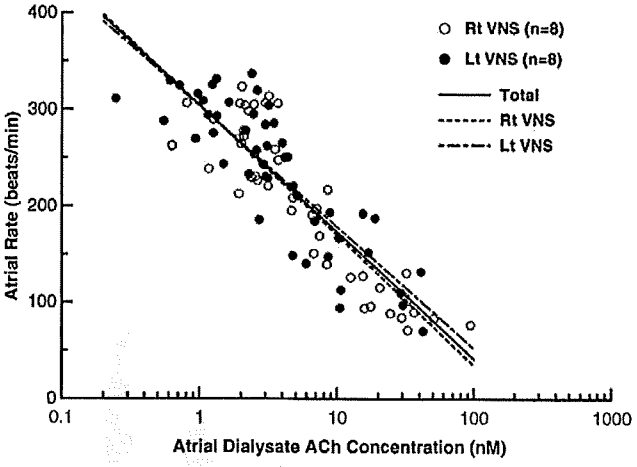

Fig. 2. Relation between dialysate ACh concentration (logarithmic scale) and atrial rate. Dialysate ACh concentration in the right atrium correlates well with atrial rate ($R^2=0.77$). Solid line, regression line fitting all 96 data points; dotted line, regression line fitting 48 data points of right vagal nerve stimulation; dot-dashed line, regression line fitting 48 data points of left vagal nerve stimulation. Rt: right; Lt: left; VNS: electrical vagal nerve stimulation.

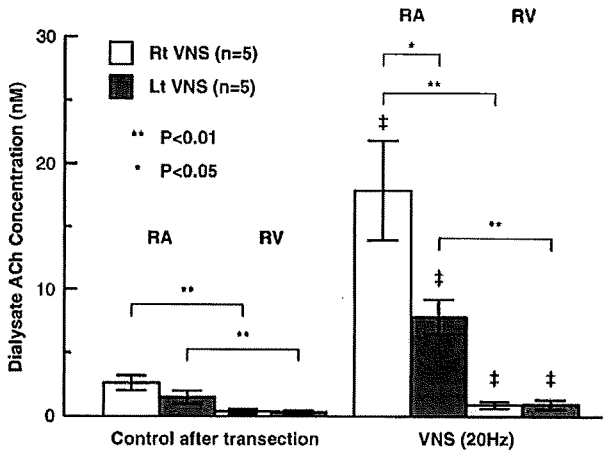

Fig. 3. Dialysate ACh concentrations in right atrium and right ventricle of controls and during electrical vagal nerve stimulation. Right vagal nerve stimulation significantly increased dialysate ACh concentration from 2.6±0.6 to 17.9±4.0 nM in the right atrium ($P<0.01$) and from 0.4±0.2 to 0.9±0.3 nM in the right ventricle ($P<0.01$). Left vagal nerve stimulation also increased dialysate ACh concentrations from 1.5±0.4 to 7.9±1.4 nM in the right atrium ($P<0.01$) and from 0.3±0.1 to 1.0±0.4 nM in the right ventricle ($P<0.01$). Dialysate ACh concentrations in the right atrium were significantly higher than those in the ventricle ($P<0.01$). Right vagal nerve stimulation increased atrial dialysate ACh concentration more than left vagal nerve stimulation ($P<0.05$). Values are means±SE; Rt: right; Lt: left; RA: right atrium; RV: right ventricle; VNS: electrical vagal nerve stimulation; *n*: number of rabbits; ‡$P<0.01$ vs. control; **$P<0.01$, *$P<0.05$.

higher during right vagal stimulation compared to left vagal stimulation ($P<0.05$).

3.3. Protocol 3

Responses of heart rate and mean arterial pressure are shown in Table 3. Both right and left vagal nerve stimulation decreased heart rate markedly before administration of hexamethonium. Administration of hexamethonium decreased heart rate significantly but mildly compared to control. Mean arterial pressure was maintained at pre-stimulation levels by continuous intravenous infusion of phenylephrine. After administration of hexamethonium, both right and left vagal nerve stimulation did not change the heart rate. Right vagal stimulation increased dialysate ACh concentration from 2.5±0.4 to 16.3±2.8 nM ($P<0.01$), but right vagal stimulation after administration of hexamethonium failed to increase ACh concentration (2.2±0.4 nM) compared to control. Likewise, left vagal stimulation increased dialysate ACh concentration from 1.5±0.3 to 8.7±1.4 nM ($P<0.01$), but left vagal stimulation after administration of hexamethonium did not increase ACh concentration (1.5±0.3 nM) compared to control (Fig. 4).

4. Discussion

We demonstrated that the microdialysis technique permitted in vivo monitoring of ACh release into the sinoatrial node from postganglionic cardiac vagal nerves. Dialysate ACh concentration in the right atrium correlated well with atrial rate and this correlation was independent of the side of vagal stimulation. These results indicate that in vivo monitoring of the myocardial interstitial ACh levels in the right atrium by microdialysis provides a useful strategy to obtain insights into the physiological roles of the vagal system in regulating heart rate.

4.1. Characteristics of atrial dialysate ACh concentration

With both right and left vagal nerve stimulation, the dialysate ACh concentration in the right atrium increased with increasing stimulus frequency and decreased to prestimulation levels after stimulation (Fig. 1). These results indicate that atrial dialysate ACh reflects ACh release from cardiac vagal nerves innervating the right atrium. Right vagal nerve stimulation decreased the atrial rate more than left stimulation at all stimulus frequencies, and right vagal nerve stimulation increased dialysate ACh concentration more than left stimulation at 10- and 20-Hz. The right atrium, including the SA node, is innervated not only by the right but also by the left vagal nerve. Ardell and Randall (1986) reported that supramaximal right and left

Table 2
Responses of heart rate and mean arterial pressure to electrical vagal nerve stimulation (protocol 2).

	Heart rate (bpm)	Mean arterial pressure (mm Hg)
Rt vagal stimulation ($n=5$)	Atrial rate (pacing rate)	
Control after transaction	305±3	74±8
VNS (20 Hz)	122±4** (304±4)	65±9*
Control after VNS	300±3	68±8
Lt vagal stimulation ($n=5$)	Atrial rate (pacing rate)	
Control after transaction	306±5	95±3
VNS (20 Hz)	168±19** (308±5)	83±1**
Control after VNS	316±8	82±2**

Values are means±SE; *n*, numbers of rabbits; Rt: right; Lt: left; VNS: electrical vagal nerve stimulation; **$P<0.01$ vs. control; *$P<0.05$ vs. control.

Table 3
Responses of heart rate and mean arterial pressure to electrical vagal nerve stimulation (protocol 3).

	Heart rate (bpm)	Mean arterial pressure (mm Hg)
Rt vagal stimulation ($n=9$)	Atrial rate (pacing rate)	
Control after transaction	292±9	70±8
VNS (20 Hz)	116±7** (299±5)	69±7
Hexamethonium iv	257±4**	84±7*
VNS after hexamethonium iv	257±4**	83±8*
Lt vagal stimulation ($n=8$)	Atrial rate (pacing rate)	
Control after transaction	317±3	79±3
VNS (20 Hz)	173±13** (313±4)	81±3
Hexamethonium iv	273±4**	87±5
VNS after hexamethonium iv	273±4**	87±4

Values are means±SE; *n*, numbers of rabbits; Rt: right; Lt: left; VNS: electrical vagal nerve stimulation; iv: intravenous administration; **$P<0.01$ vs. control; *$P<0.05$ vs. control.

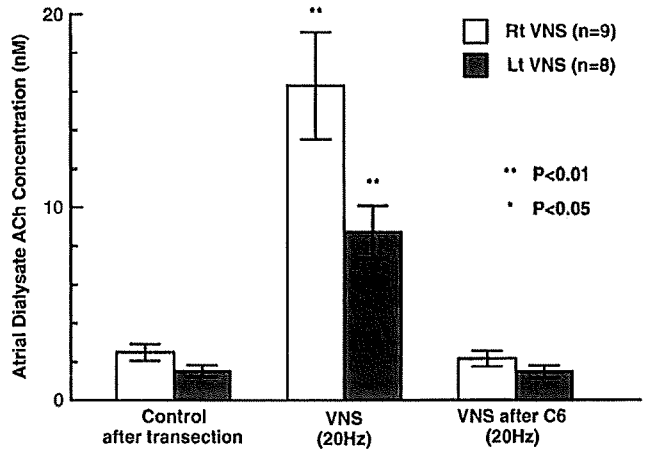

Fig. 4. Influence of ganglionic blocker on vagal nerve stimulation-induced ACh release. Right vagal nerve stimulation significantly increased atrial dialysate ACh concentration from 2.5±0.4 to 16.3±2.8 ($P<0.01$), and intravenous administration of hexamethonium suppressed the ACh concentration to 2.2±0.4 nM. Left vagal stimulation increased atrial dialysate ACh concentration from 1.5±0.3 to 8.7±1.4 nM ($P<0.01$), and hexamethonium suppressed the ACh concentration to 1.5±0.3 nM. Values are means±SE; Rt: right; Lt: left; VNS: electrical vagal nerve stimulation; C6: hexamethonium bromide; *n*: number of rabbits; **$P<0.01$ vs. control; *$P<0.05$ vs. control.

cervical vagal stimulation decreased the atrial rates to 16.3% and 48.7%, respectively, of prestimulation rates in dogs. In our study, right and left vagal stimulation at a frequency of 40 Hz also decreased the atrial rate to 30% and 42% of prestimulation rates. The difference in atrial rate response between right and left vagal nerve stimulation could be explained by the different innervation densities of the right and left vagal nerves in the right atrium including the SA node. The SA node is innervated by both right and left vagal nerves with a predominance of right vagal nerves (Ardell and Randall, 1986; Randall et al., 1985), and the response of atrial rate to vagal nerve stimulation could be ascribed to vagal ACh release into the SA node. The SA node is probably regulated by ACh released from the left as well as the right vagal nerves. In this study, dialysate ACh concentration in the right atrium (logarithmically transformed) correlated well with atrial rate, and this correlation was independent of right or left vagal stimulation (Fig. 2). These results suggest that dialysate ACh in the right atrium reflects ACh released into the SA node independent of whether the ACh originates from the right or left vagal nerves.

4.2. ACh release in atrium and ventricle

In this study, the mean dialysate ACh concentration in the right ventricle after transection of bilateral vagal nerves was 20 to 30% of that in the right atrium. During vagal nerve stimulation at 20 Hz, the atrial dialysate ACh concentration increased 5 to 7 times the control value but the ventricular dialysate ACh concentration increased to only 2 to 3 times the control value (Fig. 3). This difference between atrial and ventricular dialysate ACh concentrations could be related to the density of vagal innervation. These results are consistent with previous *in vitro* studies (Kilbinger and Löffelholz, 1976; Brown, 1976; Stanley et al., 1978). Kent et al. (1974) reported that the atrial myocardium of the vertebrate heart was richly innervated as identified by specific histochemical staining of acetylcholinesterase, in contrast to the scant innervation in the ventricular myocardium.

Right vagal nerve stimulation increased atrial dialysate ACh more than left stimulation. On the other hand, there was no difference in ventricular dialysate ACh concentration between right and left vagal nerve stimulation. Although the right atrium is predominantly innervated by the right vagal nerves, the right ventricle could be equally innervated by the right and left vagal nerves. When the right vagal nerve was stimulated at 20 Hz, heart rate decreased from 305±3 to 122±4 bpm. When the left vagal nerve was stimulated at 20 Hz, heart rate decreased from 306±5 to 169±19 bpm. This difference in heart rate response could be ascribed to vagal ACh release into the SA node. Atrial dialysate ACh concentrations were 17.9±4.0 and 7.9±1.4 nM ($P<0.05$) during stimulation of right and left vagal nerves, respectively. In contrast, there was no significant difference in ventricular dialysate ACh concentration between right and left vagal nerve stimulation. Therefore, we consider that dialysate ACh concentration in the right atrium may be a better index of ACh release into the SA node than dialysate ACh in the right ventricle.

4.3. Source of atrial dialysate ACh

In a previous study with anesthetized cats, we demonstrated that ACh in the dialysate sampled from left ventricular myocardium primarily reflects ACh released from postganglionic cardiac vagal nerves (Akiyama et al., 1994). Cardiac ganglia are located predominantly in the posterior aspect of the atria within the subepicardial connective tissue (Löffelholz and Pappano, 1985). It is possible that ACh released from stimulated preganglionic nerves contributes to ACh in the dialysate sampled from the right atrium. In this study, intravenous administration of hexamethonium bromide, a nicotinic antagonist, abolished the increase in ACh release during efferent vagal nerve stimulation. This result demonstrates that ACh in the dialysate sampled from the right atrium primarily originates from the postganglionic cardiac nerve endings.

4.4. Significance of monitoring ACh release to the SA node

Several studies have directly measured electrical efferent vagal nerve activities at the preganglionic site in vivo (Jewett, 1964; Kunze, 1972). Although this method has been used to estimate the net activity of cardiac vagal nerves, it is technically difficult to selectively measure the electrical activity of postganglionic vagal nerves innervating the SA node. Moreover, it is possible that preganglionic signals are modulated at intracardiac ganglionic sites (Gray et al., 2004). In fact, Bibevski and Dunlap (1999) have reported that attenuated vagal control in heart failure can be ascribed to attenuated ganglionic transmission. Therefore, information about postganglionic vagal nerve activity is important for understanding vagal control of heart rate.

4.5. Methodological consideration

First, we sectioned the vagi in the neck region but the sympathetic nerves were almost intact because the sympathetic nerves run separately from the vagi at the neck in rabbits. ACh released from vagal nerve terminals may interact with muscarinic receptors on postganglionic sympathetic nerve terminals to inhibit norepinephrine release prejunctionally (Levy, 1984).

Second, ACh is degraded by ACh esterase immediately after its release. Therefore to detect ACh release in vivo, addition of a specific ACh esterase inhibitor eserine into the perfusate is necessary. We used eserine at a concentration 10–100 times higher than that required in *in vitro* experimental settings because distribution of eserine across the semipermeable membrane is required, based on previous results (Akiyama et al., 1994). Eserine should spread around the semipermeable membrane, thereby affecting the ACh release in the vicinity of the dialysis membrane. Eserine may have increased the ACh level in the synaptic cleft and enhanced heart rate response by nerve stimulation, and may have also activated regulatory pathways such as autoinhibition of ACh release via muscarinic receptors.

5. Conclusion

We were able to monitor myocardial interstitial ACh levels in the right atrium around the SA node using a microdialysis technique.

Myocardial interstitial ACh level in the right atrium correlates well with atrial rate. Microdialysis combined with HPLC will become a powerful tool for understanding the parasympathetic control of heart rate.

Acknowledgements

This study was supported by Grants-in-Aid for scientific research (No. 19591829 and 20390462) from the Ministry of Education, Culture, Sports, Science and Technology; by Health and Labor Sciences Research Grants (H18-Iryo-Ippan-023, H18-nano-Ippan-003, H19-nano-Ippan-009 and H20-katsudo-Shitei-007) from the Ministry of Health, Labour and Welfare of Japan; and by the Industrial Technology Research Grant Program from New Energy and Industrial Technology Development Organization of Japan.

References

Akiyama, T., Yamazaki, T., Ninomiya, I., 1994. In vivo detection of endogenous acetylcholine release in cat ventricles. Am. J. Physiol. 266, H854–860.
Ardell, J.L., Randall, W.C., 1986. Selective vagal innervation of sinoatrial and atrioventricular nodes in canine heart. Am. J. Physiol. 251, H764–773.
Bibevski, S., Dunlap, M.E., 1999. Ganglionic mechanisms contribute to diminished vagal control in heart failure. Circulation 99, 2958–2963.
Brown, O.M., 1976. Cat heart acetylcholine: structural proof and distribution. Am. J. Physiol. 231, 781–785.
Glantz, S.A., 2005. Primer of Biostatistics, 6th ed. McGraw-Hill, New York.
Gray, A.L., Johnson, T.A., Ardell, J.L., Massari, V.J., 2004. Parasympathetic control of the heart. II. A novel interganglionic intrinsic cardiac circuit mediates neural control of heart rate. J. Appl. Physiol. 96, 2273–2278.
Jewett, D.L., 1964. Activity of single efferent fibres in the cervical vagus nerve of the dog, with special reference to possible cardio-inhibitory fibres. J. Physiol. 175, 321–357.
Kawada, T., Yamazaki, T., Akiyama, T., Shishido, T., Inagaki, M., Uemura, K., Miyamoto, T., Sugimachi, M., Takaki, H., Sunagawa, K., 2001. In vivo assessment of acetylcholine-releasing function at cardiac vagal nerve terminals. Am. J. Physiol. Heart Circ. Physiol. 281, H139–145.
Kent, K.M., Epstein, S.E., Cooper, T., Jacobowitz, D.M., 1974. Cholinergic innervation of the canine and human ventricular conducting system. Anatomic and electrophysiologic correlations. Circulation. 50, 948–955.
Kilbinger, H., Löffelholz, K., 1976. The isolated perfused chicken heart as a tool for studying acetylcholine output in the absence of cholinesterase inhibition. J. Neural Transm. 38, 9–14.
Kunze, D.L., 1972. Reflex discharge patterns of cardiac vagal efferent fibres. J. Physiol. 222, 1–15.
Levy, M.N., 1984. Cardiac sympathetic–parasympathetic interactions. Fed. Proc. 43, 2598–2602.
Löffelholz, K., Pappano, A.J., 1985. The parasympathetic neuroeffector junction of the heart. Pharmacol. Rev. 37, 1–24.
Randall, W.C., Ardell, J.L., Becker, D.M., 1985. Differential responses accompanying sequential stimulation and ablation of vagal branches to dog heart. Am. J. Physiol. 249, H133–140.
Stanley, R.L., Conaster, J., Dettbarn, W.D., 1978. Acetylcholine, choline acetyltransferase and cholinesterases in the rat heart. Biochem. Pharmacol. 27, 2409–2411.

31st Annual International Conference of the IEEE EMBS
Minneapolis, Minnesota, USA, September 2-6, 2009

Preliminary Study on the Detection of Cardiac Arrhythmias based on Multiple Simultaneous Electrograms

Telma Keiko Sugai, Student Member, *IEEE*, Makoto Yoshizawa, Member, *IEEE*,
Makoto Abe, Student Member, *IEEE*, Kazuo Shimizu, Masashi Inagaki, Member *IEEE*,
Masaru Sugimachi, Member *IEEE*, and Kenji Sunagawa, Member *IEEE*

Abstract— **Although implantable cardioverter-defibrillators have improved significantly in the past decades, the algorithms used in the identification of life-threatening arrhythmias are still not accurate enough. Conventional methods commonly misclassify tachycardias, sometimes initiating an unnecessary and uncomfortable treatment. In this paper, we proposed a new method for the identification of ventricular tachycardias and fibrillations based on the comparison of simultaneous electrograms. Our method could successfully separate supraventricular tachycardias and normal sinus rhythm, which do not require any treatment, from ventricular tachycardias and fibrillation, which are life-threatening arrhythmias and must be terminated, with a sensitivity of 93.0% and a specificity of 92.7% from the comparison of ventricular electrograms. In future studies, the classification using electrograms from the right heart must be improved.**

I. INTRODUCTION

Each year in the United States, about 450,000 people die of unexpected sudden cardiac death [1]. Further, it is known that the risk of a recurrence is high in survivors of sudden cardiac death. Therefore, in patients at risk for recurrent sustained ventricular tachycardia (VT) or fibrillation (VF), implantable cardioverter defibrillators (ICDs) are used to automatically deliver electrical shocks in order to restore the normal rhythm.

The ICDs have been used for more than 2 decades; in this period they have improved substantially becoming highly effective in terminating malignant arrhythmias. However the detection of life-threatening arrhythmias still lacks accuracy. Delivery of inappropriate shocks, commonly related to the misclassification of a supraventricular tachycardia (SVT) as a VT, can lead to pain, anxiety, depression, impaired quality of life, proarrhythmia, and poor tolerance of life-saving ICD therapy [2], [3], [4], [5], [6].

This work was supported by the Grant of Tohoku University Global COE Program: Global Nano-Biomedical Engineering Education and Research Network Center and by the Grant-In-Aid of Scientific Research of Japanese Ministry of Health, Labor and Welfare.

T.K. Sugai is with Graduate School of Biomedical Engineering, Tohoku University, 6-6-05, Aoba, Aramaki, Aoba-ku, Sendai 980-8579, Japan. telma@yoshizawa.ecei.tohoku.ac.jp

M. Yoshizawa and M. Abe are with Cyberscience Center, Tohoku University, Sendai, Japan.

K. Shimizu is with Olympus Corp., Tokyo, Japan.

M. Inagaki and M. Sugimachi are with Department of Cardiovascular Dynamics, Research Institute of National Cardiovascular Center, Osaka, Japan.

Kenji Sunagawa is with Graduate School of Medicine, Kyushu University, Fukuoka, Japan

On the other hand, the long ICD lifetime operating with typical batteries demands very low power consumption by the ICD microprocessor, which limits the use of complex detection algorithms [3].

Conventionally, ventricular arrhythmias are detected either based on the heart rate or based on the electrograms (EGMs) morphology. One example of criterion based on the heart rate is to use programmable thresholds to discriminate the arrhythmias since during a VF the heart rate is higher than during a VT, and during a VT the heart rate is higher than during a normal sinus rhythm (SR). The morphologic criterion is based on comparing the EGM morphology with a sample of pre-stored EGMs of each arrhythmia. However, both heart rate and EGM morphology are not stable, which makes it difficult to define a threshold or a particular morphology for each arrhythmia.

In this paper we propose a method for detection of ventricular arrhythmias based on the comparison of simultaneous EGMs from the left ventricle (EGM_{LV}), the right ventricle (EGM_{RV}) and the right atrium (EGM_{RA}). Preliminary results indicate that this algorithm permits earlier classification of the cardiac rhythm and with a lower computational cost than the conventional methods; however, further comparative studies are necessary. During the SR or during a SVT, the excitation is transmitted from the atrium to both ventricles through the His-Purkinje bundle; therefore, the EGM of both ventricles are synchronized with each other and with the EGM_{RA}. On the other hand, VTs and VFs are caused by an ectopic electrical excitation in the ventricle which is not transmitted through the His-Purkinje bundle causing the ventricular electrograms to be independent of each other and also of the EGM_{RA}.

II. METHODS

A. Data Description

In this study *in vivo* data were obtained from a dog in an acute experiment. EGMs were measured from leads in the left and right ventricles and right atrium and sampled at 250Hz. SVT was simulated by right atrial pacing. VT was simulated by right or left ventricular pacing. And VF was induced by electrical stimuli after the R-wave of the surface electrocardiogram. The distribution of the episodes and the length of the data of each rhythm are detailed in Table I.

978-1-4244-3296-7/09/$25.00 ©2009 IEEE

TABLE I

NUMBER OF EPISODES AND TOTAL DURATION OF THE DATA OF EACH RHYTHM

	Number of Episodes	Total Duration [s]
SR	14	179.2
SVT	5	41.6
VT	7	61.4
VF	4	40.6

B. Preprocessing

The data were analyzed in a moving data window with 1.0s length and 0.2s shift. Before the analysis, the signals were band-pass filtered between 0.8Hz and 35Hz to reduce noise and remove the baseline. Next, the relative distribution of each pair of EGMs was extracted from two dimensional histograms with 5x5 bins. In Fig. 1 are represented examples of histograms of EGM_{LV} versus EGM_{RV} for the SR and for some arrhythmias.

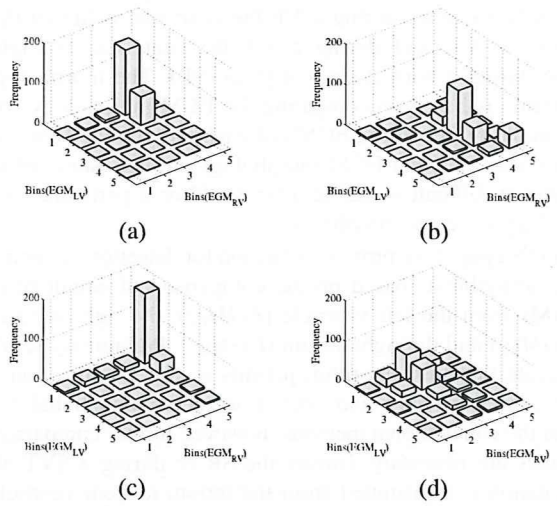

Fig. 1. Histograms representing relative distribution of EGM_{LV} and EGM_{RV} during (a) SR, (b) SVT, (c) VT and (d) VF

C. Classification

The classification was based on a decision tree using the Pearson's χ^2 statistic and the variation of the histograms. The first index was used to separate SRs and SVTs from VTs and VFs, while the second one was used to separate VTs from VFs.

The Pearson's χ^2 statistic was used to test the null hypothesis that the EGM_{LV} and the EGM_{RV}, or the EGM_{RA} and the EGM_{RV}, are independent, which is false in SRs and SVTs. The value of the test statistic χ^2 is

$$\chi^2 = \sum_{i=1}^{n_i} \sum_{j=1}^{n_j} \frac{(O_{ij} - E_{ij})^2}{E_{ij}}, \quad (1)$$

where O_{ij} is an observed frequency, E_{ij} is the expected frequency if confirmed the null hypothesis and n is the number of possible outcomes of each event.

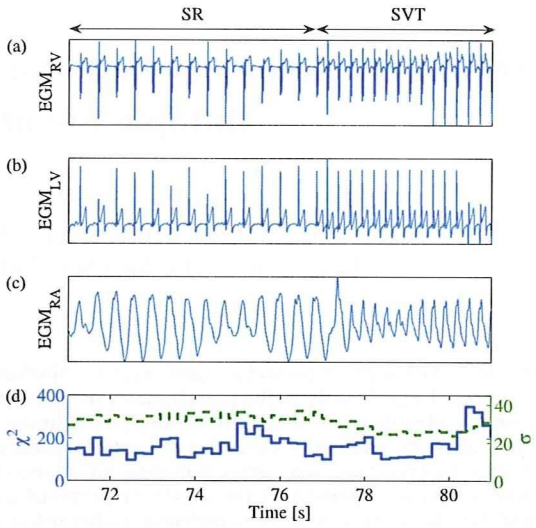

Fig. 2. Example of (a) EGM_{RV}, (b) EGM_{LV}, (c) EGM_{RA} and (d) the calculated χ^2 statistic (continuous line) and dispersion σ (dashed line) during a SVT episode.

We calculated the χ^2 using (2) approximating the joint probability distribution ($p(a_i,b_j)$) to the frequency of each bin of the histogram and the probability distribution corresponding to each EGM ($p(a_i)$ and $p(b_j)$) to the sum of the frequency of each column and each row, respectively.

$$\chi^2 = \sum_{i=1}^{5} \sum_{j=1}^{5} \frac{(p(a_i,b_j) - p(a_i) \cdot p(b_j))^2}{p(a_i) \cdot p(b_j)}. \quad (2)$$

Next, the dispersion of the histogram of two EGMs was used to identify VFs. The dispersion of the histogram was calculated as the standard deviation (σ) of the counts in each bin of the histogram, as in (3).

$$\sigma = \frac{1}{n_a \cdot n_b} \sum_{i=1}^{n_a} \sum_{j=1}^{n_b} (p(a_i,b_j) - \mu)^2, \quad (3)$$

where μ is the mean of $p(a_i,b_j)$.

The classification was validated using a 10-fold cross validation. The training and validation sets were separated maintaining a constant rate of 9:1 samples of each rhythm. The thresholds were interactively defined as the value that maximizes the sensitivity and the specificity of the classification of the training set.

III. RESULTS

Figs. 2, 3 and 4 show examples of EGMs and the calculated indices during the transition to a SVT, a VT and a VF episode, respectively. In the top three graphs ((a), (b) and (c)) of each figure are represented segments of EGMs acquired simultaneously from the right ventricle, left ventricle and right atrium. In the bottom graph (d) of each figure are shown the values of the indices used for the classification: χ^2-statistic and σ, extracted from the ventricular EGMs represented in the top graphs.

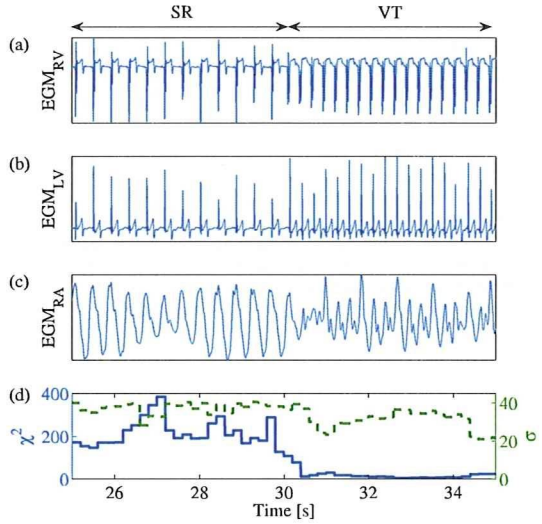

Fig. 3. Example of (a) EGM_{RV}, (b) EGM_{LV}, (c) $EGM_{RA}$and (d) the calculated χ^2 statistic (continuous line) and dispersion σ (dashed line) during a VT episode.

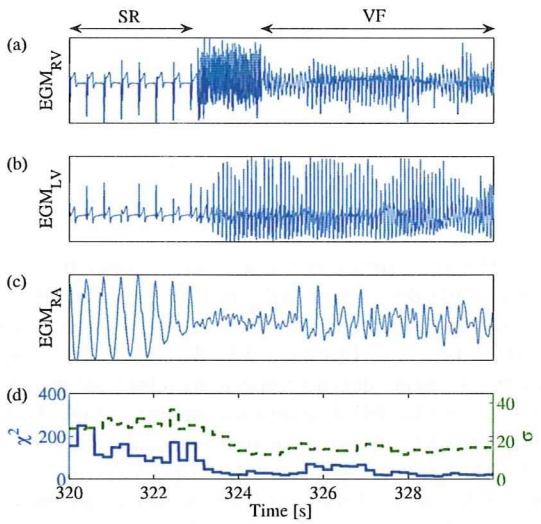

Fig. 4. Example of (a) EGM_{RV}, (b) EGM_{LV}, (c) $EGM_{RA}$and (d) the calculated χ^2 statistic (continuous line) and dispersion σ (dashed line) during a VF episode.

TABLE II

PERFORMANCE OF THE CLASSIFIER USING EGM_{LV} AND EGM_{RV} (VENTRICULAR ARRHYTHMIAS VS. OTHER RHYTHMS)

	VT or VF	SR or SVT
Shock	TP = 549	FP = 86
Ignore	FN = 41	TN = 1104
	Sensitivity = 93.0%	Specificity = 92.7%

TABLE III

PERFORMANCE OF THE CLASSIFIER USING EGM_{LV} AND EGM_{RV} (VT VS. VF)

	VF	VT
Shock	TP = 229	FP = 7
Pacing	FN = 10	TN = 303
	Sensitivity = 95.8%	Specificity = 97.7%

The results from the validation of the classifier are shown in Tables II - V. In the classification using both ventricular EGMs, EGM_{LV} and EGM_{RV}, the mean ($\pm$ standard deviation) threshold for the χ^2 was 76.4 ($\pm$ 1.9) and the mean threshold for the σ was 16.8 ($\pm$ 0.3). In the classification using ECGs from the right heart, EGM_{RA} and EGM_{RV}, the mean ($\pm$ standard deviation) threshold for the χ^2 was 61.1 ($\pm$ 0.9) and the mean threshold for the σ was 13.2 ($\pm$ 0.2).

The sensitivity and specificity of the classifier were calculated from the sum of the respective true positive (TP), false positive (FP), false negative (FN) and true negative (TN) of each interaction of the cross validation. The detailed results of the detection of life-threatening arrhythmias, by separating VTs and VFs from SVTs and SRs, are shown in Tables II and IV. The results of the decision of whether the ICD should apply a shock to recover from a VF, or start pacing to recover from a VT, are detailed in Tables III and V.

The results presented in Tables II and III correspond to the classification based on the EGM_{LV} and the EGM_{RV}, which are available only in biventricular ICDs. The results presented in Tables IV and V correspond to the classification based on the EGM_{RA} and the EGM_{RV}, which are available also in dual chamber ICDs.

IV. DISCUSSION

Conventional methods for the discrimination of the cardiac rhythms have a special limitation for the separation between SVTs and VTs. Studies using morphology-based algorithms have reported higher specificity and sensitivity in this detection, however it was still necessary to have a more accurate method that could fit the low computational cost requirements of an ICD [5].

In this paper, we proposed a new algorithm for the detection of arrhythmias for ICDs. On the basis of the comparison of EGMs, VF and VT were separated from SVT or SR by the comparison of the independence of the two simultaneous EGMs. It was observed that during the normal SR, and also during SVT, there was a high similarity especially between the EGM_{LV} and the EGM_{RV}, which decreased during ventricular arrhythmias. Dependencies are commonly measured using mutual information or χ^2 statistics; in this study, we

TABLE IV

PERFORMANCE OF THE CLASSIFIER USING EGM_{RA} AND EGM_{RV} (VENTRICULAR ARRHYTHMIAS VS. OTHER RHYTHMS)

	VT or VF	SR or SVT
Shock	TP = 439	FP = 318
Ignore	FN = 151	TN = 872
	Sensitivity = 74.4%	Specificity = 73.3%